Implications of *TP53* Allelic State for Genome Stability, Clinical Presentation and Outcomes in Myelodysplastic Syndromes

Elsa Bernard[1,2], Yasuhito Nannya[3], Robert P. Hasserjian[4], Sean M. Devlin[5], Heinz Tuechler, Juan S. Medina-Martinez[1,2], Tetsuichi Yoshizato[3], Yusuke Shiozawa[3], Ryunosuke Saiki[3], Luca Malcovati[6,7], Max F. Levine[1,2], Juan E. Arango[1,2], Yangyu Zhou[1,2], Francesc Sole[8], Catherine A. Cargo[9], Detlef Haase[10], Maria Creignou[11], Ulrich Germing[12], Yanming Zhang[13], Gunes Gundem[1], Araxe Sarian[2], Arjan A. van de Loosdrecht[14], Martin Jädersten[11], Magnus Tobiasson[11], Olivier Kosmider[15], Matilde Y. Follo[16], Felicitas Thol[17], Ronald F. Pinheiro[18], Valeria Santini[19], Ioannis Kotsianidis[20], Jacqueline Boultwood[21], Fabio P.S. Santos[22], Julie Schanz[10], Senji Kasahara[23], Takayuki Ishikawa[24], Hisashi Tsurumi[25], Akifumi Takaori-Kondo[26], Toru Kiguchi[27], Chantana Polprasert[28], John M. Bennett[29], Virginia M. Klimek[30], Michael R. Savona[31], Monika Belickova[32], Christina Ganster[10], Laura Palomo[8], Guillermo Sanz[33,34], Lionel Ades[35], Matteo Giovanni Della Porta[36], Alexandra G Smith[37], Yesenia Werner[1], Minal Patel[2], Agnès Viale[38], Katelynd Vanness[38], Donna S. Neuberg[39], Kristen E. Stevenson[39], Kamal Menghrajani[30], Kelly L. Bolton[30], Pierre Fenaux[35], Andrea Pellagatti[21], Uwe Platzbecker[40], Michael Heuser[17], Peter Valent[41], Shigeru Chiba[42], Yasushi Miyazaki[43], Carlo Finelli[44], Maria Teresa Voso[45], Lee-Yung Shih[46], Michaela Fontenay[15], Joop H. Jansen[47], José Cervera[48], Yoshiko Atsuta[49], Norbert Gattermann[12], Benjamin L. Ebert[50], Rafael Bejar[51], Peter L. Greenberg[52], Mario Cazzola[6,7], Eva Hellström-Lindberg[11], Seishi Ogawa*[3] and Elli Papaemmanuil*[1,2]

*Shared senior authorship

Affiliations:

[1]Computational Oncology Service, Department of Epidemiology & Biostatistics, Memorial Sloan Kettering Cancer Center, New York, NY, USA.
[2]Center for Hematologic Malignancies, Memorial Sloan Kettering Cancer Center, New York, NY, USA.
[3]Department of Pathology and Tumor Biology, Kyoto University, Kyoto, Japan.
[4]Department of Pathology, Massachusetts General Hospital, Boston, MA, USA.
[5]Department of Epidemiology & Biostatistics, Memorial Sloan Kettering Cancer Center, New York, NY, USA.
[6]Department of Molecular Medicine, University of Pavia, Pavia. Italy.
[7]Department of Hematology, IRCCS Fondazione Policlinico S. Matteo, Pavia. Italy.
[8]MDS Group, Institut de Recerca Contra la Leucèmia Josep Carreras, Barcelona, Spain.
[9]Haematological Malignancy Diagnostic Service, St James's University Hospital, Leeds, United Kingdom.
[10]Clinics of Hematology and Medical Oncology, University Medical Center. Göttingen, Germany.
[11]Department of Medicine Huddinge, Center for Hematology and Regenerative Medicine, Karolinska Institutet, Karolinska University Hospital, Stockholm, Sweden.
[12]Department of Hematology, Oncology and Clinical Immunology, Heinrich Heine University, Düsseldorf, Germany.
[13]Department of Pathology, Memorial Sloan Kettering Cancer Center, New York, NY, USA.
[14]Department of Hematology, VU University Medical Center Amsterdam, The Netherlands.
[15]Department of Hematology, Assistance Publique-Hôpitaux de Paris, Hôpital Cochin and Université de Paris, Université Paris Descartes, Paris, France.
[16]Department of Biomedical and Neuromotor Sciences, University of Bologna, Bologna, Italy.
[17]Department of Hematology, Hemostasis, Oncology and Stem Cell Transplantation, Hannover Medical School, Hannover, Germany.
[18]Drug Research and Development Center, Federal University of Ceara, Ceara, Brazil.

[19]MDS Unit, Hematology, AOU Careggi, University of Florence, Italy.
[20]Department of Hematology, Democritus University of Thrace Medical School, Alexandroupolis, Greece.
[21]Radcliffe Department of Medicine, University of Oxford and Oxford BRC Haematology Theme, Oxford, United Kingdom.
[22]Oncology-Hematology Center, Hospital Israelita Albert Einstein, São Paulo, Brazil.
[23]Department of Hematology, Gifu Municipal Hospital, Gifu, Japan.
[24]Department of Hematology, Kobe City Medical Center General Hospital, Kobe, Japan.
[25]Department of Hematology, Gifu University Graduate School of Medicine, Gifu, Japan.
[26]Department of Hematology and Oncology, Graduate School of Medicine, Kyoto University, Japan.
[27]Department of Hematology, Chugoku Central Hospital, Fukuyama, Japan.
[28]Department of Medicine, Chulalongkorn University, King Chulalongkorn Memorial Hospital, Bangkok, Thailand.
[29]Lab. Medicine and Pathology, Hematology/Oncology, University of Rochester Medical Center, Rochester, NY, USA.
[30]Department of Medicine, Memorial Sloan Kettering Cancer Center, New York, NY, USA.
[31]Department of Medicine, Vanderbilt-Ingram Cancer Center, Vanderbilt University School of Medicine, Nashville, TN, USA.
[32]Department of Genomics, Institute of Hematology and Blood Transfusion, Prague, Czech Republic.
[33]Department of Hematology, Hospital Universitario y Politécnico La Fe, Valencia, Spain.
[34]CIBERONC, Instituto de Salud Carlos III, Madrid, Spain.
[35]Department of Hematology, hôpital St Louis, and Paris University, Paris, France.
[36]Cancer Center, Humanitas Research Hospital & Humanitas University, Milan Italy.
[37]Department of Health Sciences, University of York, United Kingdom.
[38]Integrated Genomics Operation, Memorial Sloan Kettering Cancer Center, New York, NY, USA.
[39]Department of Data Sciences, Dana-Farber Cancer Institute, Boston, MA, USA.
[40]Medical Clinic and Policlinic 1, Hematology and Cellular Therapy, University of Leipzig, Leipzig, Germany.
[41]Department of Internal Medicine I, Division of Hematology and Hemostaseology and Ludwig Boltzmann Institute for Hematology and Oncology, Medical University of Vienna, Austria.
[42]Department of Hematology, Faculty of Medicine, University of Tsukuba, Tsukuba, Japan.
[43]Department of Hematology, Atomic Bomb Disease Institute, Nagasaki University, Japan.
[44]Institute of Hematology, S.Orsola-Malpighi University Hospital, Bologna, Italy.
[45]MDS Cooperative Group GROM-L, Department of Biomedicine and Prevention, Tor Vergata University, Rome, Italy.
[46]Chang Gung Memorial Hospital at Linkou, Chang Gung University, Taiwan.
[47]Laboratory Hematology, Department LABGK, Radboud University Medical Centre, Nijmegen, The Netherlands.
[48]Department of Hematology and Genetics Unit, University Hospital La Fe, Valencia, Spain.
[49]Japanese Data Center for Hematopoietic Cell Transplantation, Nagoya, Japan.
[50]Department of Medical Oncology and Howard Hughes Medical Institute, Dana-Farber Cancer Center, Boston, MA, USA.
[51]UC San Diego Moores Cancer Center, La Jolla, California, USA.
[52]Stanford University Cancer Institute, Stanford, CA, USA.

Address for correspondence: papaemme@mskcc.org

_TP53_ is the most frequently mutated gene in cancer[1,2]. In patients with myelodysplastic syndromes (MDS), _TP53_ mutations are associated with high-risk disease[3,4], rapid transformation to acute myeloid leukemia (AML)[5], resistance to conventional therapies[6,7,8] and dismal outcomes[9]. Consistent with the tumor suppressive role of _TP53_, patients harbor both mono- and bi-allelic mutations[10]. However, the biological and clinical implications of _TP53_ allelic state have not been fully investigated in MDS or any other cancer type. We analyzed 3,324 MDS patients for _TP53_ mutations and allelic imbalances and delineated two subsets of patients with distinct phenotypes and outcomes. One third of _TP53_-mutated patients had mono-allelic mutations whereas two third had multiple hits (multi-hit) consistent with bi-allelic targeting. Established associations with complex karyotype, few co-occurring mutations, high-risk presentation and poor outcomes were specific to multi-hit patients only. _TP53_ multi-hit state predicted risk of death and leukemic transformation independently of the Revised International Prognostic Scoring System (IPSS-R)[11]. Surprisingly, mono-allelic patients did not differ from _TP53_ wild-type patients in outcomes and response to therapy. This study shows that consideration of _TP53_ allelic state is critical for diagnostic and prognostic precision in MDS as well as future correlative studies of treatment response.

In collaboration with the International Working Group for Prognosis in MDS (Supplementary Table 1) we assembled a cohort of 3,324 peri-diagnostic and treatment naive patients with MDS or closely related myeloid neoplasms (Extended Data Table 1 and Supplementary Fig. 1). Genetic profiling included conventional G-banding analyses (CBA) and tumor only capture based next generation sequencing (NGS) of a panel of genes recurrently mutated in MDS, as well as genome wide copy-number probes. Allele specific copy-number profiles were generated from NGS data using CNACS[7] (see Methods and Code availability). An additional 1,120 samples derived from the Japanese MDS consortium (Extended Data Table 2) were used as a validation cohort.

To study the effect of *TP53* allelic state on genome stability, clinical presentation, outcome and response to therapy, we performed a detailed characterization of alterations at the *TP53*

locus. First, we assessed genome wide allelic imbalances in the 3,324 patients, to include arm level or focal (~3Mb) ploidy alterations and regions of copy neutral loss of heterozygosity (cnLOH) (Extended Data Fig. 1, Supplementary Fig. 2-4 and Methods). Collectively, 360 (11%) patients had at least one cnLOH region and 1,571 (47%) had ≥1 chromosomal aberration. Among these, 329 karyotypes were complex[12] and 177 were monosomal[13] (Supplementary Table 2).

Mutation analysis identified 486 putative oncogenic mutations in *TP53* at variant allele frequency (VAF) ≥2% across 378 individuals (Supplementary Fig. 5-7 and Methods). Among *TP53*-mutant patients, 274 (72.5%) had a single *TP53* mutation, 100 had two (26.5%) and 4 (1%) had three. Allelic imbalances overlapping the *TP53* locus were found in 177 cases. Of these, 98 were focal deletions or regions of cnLOH detected by NGS only (Supplementary Table 3). Approximately half (54%, n=149) of patients with one *TP53* mutation had loss of the wild-type allele by deletion or cnLOH. In contrast, only 13% (n=14) of patients with ≥2 *TP53* mutations had a concomitant allelic imbalance at the *TP53* locus (OR=8, $p<10^{-13}$ Fisher exact test) (Fig. 1a). By consideration of mutations and allelic imbalances, we defined 4 *TP53*-mutant subgroups (Fig. 1b): 1. Mono-allelic mutation (n=125, 33% of *TP53*-mutated patients); 2. Multiple mutations without deletion or cnLOH affecting the *TP53* locus (n=90, 24%); 3. Mutation(s) and concomitant deletion (n=85, 22%); 4. Mutation(s) and concomitant cnLOH (n=78, 21%). Additionally, in 24 patients, the *TP53* locus was affected by deletion (n=12), cnLOH (n=2) or isochromosome 17q rearrangement (n=10) without evidence of *TP53* mutations (Fig. 1a).

In subgroups 2-4, clonality estimates of co-occurring mutations or allelic imbalances supported bi-allelic targeting of *TP53* (Extended Data Fig. 2). In a subset of cases, bi-allelic targeting was validated by phasing analysis or sequential sampling (Supplementary Fig. 8). Thus, the *TP53*-mutant subgroups were organized into two states: A. mono-allelic *TP53* state representing subgroup 1, with one residual wild-type copy of *TP53* and B. multi-hit *TP53* state encompassing subgroups 2-4, with at least two *TP53* hits in each patient and likely no residual *TP53*. While most multi-hit samples were confidently "bi-allelic" we maintained a conservative "multi-hit" notation.

Accurate determination of allelic state requires LOH mapping, as can be achieved by NGS-based analysis of sequencing panels[7] or more comprehensive sequencing methods (Supplementary Fig. 4). VAF estimates were not sufficient to precisely assess *TP53* allelic state (Fig. 1c). For example, 19 cnLOH-positive patients had *TP53* VAF ≤50% (median 29%, range 3-49%), showing that ¼ of cnLOH patients would be mis-assigned as mono-allelic on the basis of VAF.

In mono-allelic cases, *TP53* mutations were enriched for subclonal presentation (median VAF: 13%, median sample purity: 86%) as compared to *TP53* mutations from patients with multiple mutations which were predominantly clonal (median VAF: 32%, median sample purity: 85%) (Fig. 1c). Thus, *TP53* allelic state, and by extension whether a wild-type *TP53* allele is retained, points towards different evolutionary trajectories or potential for clonal dominance. Overall, the spectrum of *TP53* mutations was shared among the two allelic states (Fig. 1d and Supplementary Fig. 9). Of note, truncating mutations were enriched in the multi-hit state (28% vs. 14%, OR=2.3, p=0.002 Fisher exact test) while hotspot mutations accounted for 25% of mutations in the mono-allelic state and 20% in the multi-hit state (OR=1.38, p=0.2).

We next assessed profiles of genome stability and patterns of co-mutations for each *TP53* state. The correlation between *TP53* mutations and chromosomal aneuploidies is well established[3,7,14,15,16]. Overall, 67% (n=252) of *TP53*-mutated cases had ≥2 chromosomal deletions as compared to 5% (n=158) of wild-type cases (OR=35, $p<10^{-16}$ Fisher exact test). Excluding chr17 (which is linked to state definition), there was a significantly higher number of chromosomal aberrations per patient in all multi-hit *TP53* subgroups compared to the mono-allelic group (Fig. 2a and Extended Data Fig. 3). This enrichment was most pronounced for deletions (median 4 in multi-hit vs. 1 in mono-allelic state, $p<10^{-16}$ Wilcoxon rank-sum test). In particular, deletion of 5q was observed in 85% of multi-hit patients as opposed to 34% of mono-allelic patients (OR=10, $p<10^{-16}$ Fisher exact test, Supplementary Fig. 10). Taken together, we found a median of 6 unique chromosomes with aberrations in the multi-hit state and 1 in the mono-allelic state ($p<10^{-16}$ Wilcoxon rank-sum test, Fig. 2b). Our data suggest that residual wild-type *TP53* is critical to maintenance of genome stability, and that the association between

TP53 and complex karyotype is specific to the multi-hit state (91% vs. 13% complex karyotype patients within multi-hit or mono-allelic states, OR=70, $p<10^{-16}$ Fisher exact test, Fig. 2c).

The total number of oncogenic gene mutations and the pattern of co-mutations were also different among the allelic states. Excluding *TP53*, the number of driver mutations was higher in the mono-allelic state compared to the multi-hit *TP53* subgroups (Fig. 2d). Overall, 40% (n=102) of multi-hit patients did not have any identifiable driver mutations other than *TP53*, while 90% (n=112) of mono-allelic patients had at least one other driver mutation and 50% (n=62) had at least three. Differences in the pattern of co-mutations were also identified, whereby mono-allelic patients were significantly enriched for mutations in *TET2*, *SF3B1*, *ASXL1*, *RUNX1*, *SRSF2*, *JAK2*, *BCOR* and *CBL* (Fig. 2e).

Prior studies have recurrently linked *TP53* mutations to high-risk presentation (complex karyotype, elevated blasts, severe thrombocytopenia) and adverse outcomes[3,4]. These correlations were recapitulated in our study (Supplementary Fig. 11). However, the clinical implications of the allelic state have not been investigated. In our cohort, mono-allelic *TP53* patients were less cytopenic (Fig. 3a-c) and had lower percentages of bone marrow blasts compared to multi-hit patients (median 4 vs. 9%, $p<10^{-10}$ Wilcoxon rank sum test, Fig. 3d). There was a higher prevalence of lower risk MDS in mono-allelic patients, while the multi-hit state was enriched for higher risk WHO subtypes and poor/very-poor IPSS-R categories (Extended Data Fig. 4a-b). Overall survival (OS) and AML transformation were significantly different between the *TP53* allelic states. In multi-hit state, the median OS was 8.7 months (95% CI: 7.7-10.3 months) whereas it was 2.5 years (95% CI: 2.2-4.9 years) for mono-allelic patients (HR=3.7, 95% CI: 2.7-5.0, $p<10^{-16}$ Wald test). In comparison, wild-type patients had a median OS of 3.5 years (95% CI: 3.4-3.9 years) (Fig. 3e). The effect of mono-allelic *TP53* on OS was not confounded by del(5q) (Supplementary Fig. 12). The 5-year cumulative incidence of AML transformation in the multi-hit and mono-allelic states were respectively 44% and 21% (HR=5.5, 95% CI: 3.1-9.6, $p<10^{-8}$ Wald test) (Fig. 3f). Of note, all subgroups (>1 gene mutations, mutation and deletion, mutation and cnLOH) in multi-hit state had equally dismal outcomes (Extended Data Fig. 5a-b). The OS distinction of the two states was significant across WHO classes and IPSS-R risk groups (Extended Data Fig. 4c-d and Supplementary Fig. 13), and multi-hit *TP53* identified patients with

poor survival across IPSS-R strata. As 10% of multi-hit patients were classified as IPSS-R very-good to intermediate risk, this shows that assessment of *TP53* allelic state is critical to identify patients with high-risk disease. In fact, multivariable Cox proportional hazards models that included *TP53* state alongside age of diagnosis, cytogenetic risk score[12] and established predictive features identified multi-hit *TP53* as an independent predictor for the risk of death and AML transformation (HR_{OS}=2.04, 95% CI: 1.6-2.6, $p<10^{-7}$; HR_{AML}=2.9, 95% CI: 1.8-4.7, $p<10^{-5}$ Wald test), whereas mono-allelic *TP53* state was not different compared to wild-type *TP53* (Fig. 3g-h). We also evaluated that multi-hit *TP53* and complex karyotype, but not mono-allelic *TP53*, were independent predictors of adverse outcome (Supplementary Fig. 15), emphasizing the importance of mapping *TP53* state alongside complex karyotype for accurate risk estimation.

Outcomes of mono-allelic patients significantly differed with the number of co-occurring driver mutations (Fig. 2d-e and Supplementary Fig. 14). For example the 5-year survival rate of mono-allelic patients without any other identifiable mutations was 81%, while it was 36% for patients with 1 or 2 other mutations, 26% for patients with 3 or 4 other mutations and 8% for patients with more than 5 other mutations. Contrastingly, the outcome of multi-hit patients did not depend on the number of additional mutations, and the 5-year survival rate was uniformly below 6%. Taken together, multi-hit *TP53* patients had few co-mutations and very poor survival irrespective of genetic context. Patients with mono-allelic *TP53* mutations frequently had several co-occurring mutations which shaped disease pathogenesis and outcomes. This data further showcased that mono-allelic *TP53* mutations were not independently predictive of adverse risk.

In addition to *TP53* mutations, *TP53* VAF has also been reported to be of prognostic significance in MDS[17,18,19]. This is likely explained by the strong correlation between high VAF and bi-allelic targeting. Optimal cut-point analysis[20] identified that patients with mono-allelic *TP53* mutations and VAF>22% (n=38) had increased risk of death compared to wild-type patients (HR=2.2, 95% CI: 1.5-3.2, $p<10^{-4}$ Wald test), whereas patients with mono-allelic *TP53* mutations and VAF≤22% (n=87) had similar OS than wild-type patients (Extended Data Fig. 5c). This highlights that patients with mono-allelic mutations and high VAF should be closely monitored. It is possible that we have missed a second *TP53* hit in the small subset of mono-allelic cases with VAF>22%. Conversely, multi-hit patients had poor outcomes across ranges of VAF. Patients with

low VAF≤11% (n=20) had very dismal outcomes, for both OS and AML transformation (Extended Data Fig. 5c-d). Importantly, the genomic and clinical associations established for multi-hit cases held true irrespective of VAF. Patients with multi-hit *TP53* had higher genome instability, fewer cooperating mutations, more pronounced thrombocytopenia and elevated blast counts compared to mono-allelic patients in both clonal and subclonal ranges (Supplementary Fig. 16). This indicates that, once established, a clone with bi-allelic *TP53* targeting exerts its pervasive effects on clinical phenotypes and outcomes regardless of its size. The determination of *TP53* allelic state requires assessment of both multiple mutations and subclonal allelic imbalances, and multi-hit *TP53* state identified very high-risk patients independently of the VAF of *TP53* mutations.

The emergence of data in support of dominant negative effect (DNE)[21,22] and gain of function (GOF)[23,24,25] led us to test whether outcomes differed based on the nature of the underlying lesion, i.e., missense, truncated or hotspot *TP53* mutations. In the multi-hit state, no differences were observed on genome instability and outcomes across mutation types (Extended Data Fig. 6 and Supplementary Fig. 17a-b), indicating that it is the loss of both wild-type copies of *TP53* that drives the dismal outcomes of *TP53*-mutated MDS patients rather than the underlying mutation types. In the mono-allelic state, missense mutations in the DNA binding domain (DBD) had no effect on patient outcomes compared to wild-type *TP53*. However, there was an increased risk of death of mono-allelic patients with hotspot mutation at amino acid positions R175 and R248 (but not R273) compared to wild-type patients (HR=2.3, 95% CI: 1.2-4.7, p=0.02 for R248 and HR=3.0, 95% CI: 0.96-9.3, p=0.06 Wald test for R175, Supplementary Fig. 17c-d), consistent with either DNE[21] or GOF[25] of the hotspot mutant proteins. This suggests that DNE[21] may not be applicable to all DBD mutations, especially in the setting of MDS where exposure to genotoxic therapy is not common. Larger datasets and functional studies are warranted to further investigate the operative mechanisms of DBD mutations in MDS.

Beyond primary MDS, *TP53* mutations are enriched in therapy-related MDS (t-MDS)[6,26] and are associated with a high-risk of progression to AML[5]. In t-MDS and at progression, *TP53*-mutated patients demarcate an extremely adverse prognostic group with a chemo-refractory disease and less than 2% 5-year survival[15,16]. Our cohort included 229 t-MDS

cases, with a higher proportion of *TP53*-mutated patients relative to de-novo MDS (18% vs. 6%, OR=3.3, $p<10^{-11}$ Fisher exact test). *TP53*-mutated t-MDS patients more frequently had multiple hits compared to *TP53*-mutated de-novo patients (84% vs. 65%, OR=2.8, p=0.002). Comparison of genome profiles (Supplementary Fig. 18) and clinical outcomes (Fig. 4a) between allelic states reiterated observations from de-novo MDS. *TP53*-mutant t-MDS is considered one of the most lethal malignancies with limited treatment options[27], yet mono-allelic patients had lower risk of death compared to multi-hit patients (HR=0.39, 95% CI: 0.15-1.0, p=0.05 Wald test).

To evaluate the effect of *TP53* state in disease progression, we analyzed serial data from 12 MDS patients of an independent cohort[28,29] (St James's University Hospital, United Kingdom) who progressed to AML with a *TP53* mutation (Supplementary Fig. 19). In 7/12 patients, multiple hits were observed at time of MDS diagnosis, with a 4 months median to AML progression (Supplementary Fig. 19a-g). In 3 patients, bi-allelic targeting occurred during disease progression with inter-clonal competition and attainment of clonal dominance for the *TP53* clone (Supplementary Fig. 19h-i). The remaining two cases that progressed with a mono-allelic *TP53* mutation had other high-risk mutations in *RUNX1* and *KRAS* or in *CBL* (Supplementary Fig. 19k-l), consistent with the observation from our discovery cohort that mono-allelic *TP53* mutations tend to occur with several and diverse cooperating mutations (Fig. 2d-e). These data provided further evidence that bi-allelic alteration of *TP53* is a potent driver of disease progression and underscore the importance of assessing *TP53* allelic state at diagnosis and for disease surveillance.

We validated the representation of *TP53* allelic states (Supplementary Fig. 20), genome stability profiles (Supplementary Fig. 21) and differences in clinical phenotypes (Supplementary Fig. 22) in a cohort of 1,120 MDS patients (Extended Data Table 2).

Last, we evaluated the implication of *TP53* allelic state in response to therapy. Recent studies reported that *TP53* patients have poor responses to lenalidomide[8] and HSCT[6,7], as well as marked but transient responses to hypomethylating agent (HMA)[30]. We conducted an exploratory survival analysis by allelic state for patients that received HMA, lenalidomide on the subset with del(5q) and following HSCT (Extended Data Table 3). On HMA and lenalidomide,

patients with mono-allelic *TP53* mutations had evidence of longer survival compared to multi-hit patients (Fig. 4b-c). The analysis of our HSCT cohort was limited due to its size, yet we observed a trend for improved survival of mono-allelic patients compared to multi-hit patients following HSCT (Fig. 4d). These observations highlight the importance of mapping *TP53* allelic states in future correlative studies of response to therapy.

In summary, we provided a detailed characterization of *TP5*3 allelic state in 3,324 MDS patients and assessed its implication for disease biology, clinical presentation and outcomes. Two third of *TP53*-mutated patients had multiple hits (>1 gene mutations, mutation and deletion, mutation and cnLOH) consistent with bi-allelic targeting. The remaining third had mono-allelic mutations with one residual wild-type allele.

We demonstrated that the multi-hit *TP53* state in MDS, not the bare presence of any *TP53* mutation, underlies established associations with genome instability, treatment resistance, disease progression and dismal outcomes. Multi-hit *TP53* identified very high-risk patients independently of the IPSS-R, co-occurring mutations and clonal representation. Surprisingly, mono-allelic *TP53* patients did not differ from *TP53* wild-type patients with regards to response to therapy, overall survival and AML progression. The shift in survival for mono-allelic patients with the number of co-mutations indicates diversity of disease pathogenesis and highlights the need for prognostic models that consider a large spectrum of gene mutations in the future.

Different evolutionary trajectories between multi-hit and mono-allelic patients emerged from our data. In multi-hit state, *TP53* mutations were predominantly in the dominant clone with complex karyotypes and few other mutations, reflecting early truncal events in MDS pathogenesis. In contrast, mono-allelic *TP53* mutations were frequently subclonal and co-occurred with mutations from a broad range of genes, to include genes associated with both a favorable[31] (*SF3B1*) or poor[32] (*ASXL1*, *RUNX1, CBL*) prognosis. A limitation of our study is that we may have missed a second hit for a small subset of cases, such as balanced rearrangement or aberrant methylation. However, the systematic differences between mono-allelic and multi-hit patients across genomic and clinical metrics indicate that our definition of *TP53* allelic state

delineates two biologically and clinically relevant groups. In Extended Data Fig. 7, we propose a workflow to map *TP53* allelic state in routine diagnostic practice.

Our findings imply that diagnostic and prognostic precision in MDS requires the assessment of *TP53* allelic state. We propose that bi-allelic *TP53* should be distinguished from mono-allelic *TP53* mutations in future revisions of the IPSS-R and in correlative studies of treatment response. As the most frequently mutated gene in cancer, the representation and effect of *TP53* allelic state warrant investigation across cancer indications.

ONLINE METHODS

Patient samples

The International Working Group for Prognosis in MDS (IWG-PM) cohort originated from 24 MDS centers (Supplementary Table 1) that contributed peri-diagnosis MDS, MDS/MPN and AML/AML-MRC patient samples to the study. Upon quality control (Supplementary Fig. 1), 3,324 samples were included in the study (Extended Data Table 1). The source for genomic DNA was bone marrow or peripheral blood mononuclear cells. The median time from diagnosis to sampling was 0 days (1st quartile: 0 days, 3rd quartile: 113 days). The validation cohort consisted of 1,120 samples from the Japanese MDS consortium (Extended Data Table 2). Samples were obtained with informed consent in accordance with the Declaration of Helsinki and appropriate Ethics Committee approval.

Clinical data

Diagnostic clinical variables were provided by the contributing centers and curated to ensure uniformity of metrics across centers and countries. Clinical variables included i) Sex ii) Age at diagnosis iii) WHO disease subtype iv) MDS type i.e., de-novo, secondary or therapy-related MDS v) Differential blood counts to include hemoglobin, platelets, white blood cell, neutrophil and monocyte vi) Percentage of bone marrow and peripheral blood blasts vii) Cytogenetic data and viii) Risk score as per IPSS-R[11]. Clinical outcomes included the time of death from any cause or last follow-up from sample collection, and the time of AML transformation or last follow-up from sample collection.

Cytogenetic data

Conventional banding analysis (CBA) data were available for 2,931 patients and karyotypes were described in accordance with the International System for Human Cytogenetic Nomenclature[33]. CBA data were risk stratified according to the IPSS-R guidelines[12] using both algorithmic classification and manual classification by an expert panel of cytogeneticists.

WHO subtypes

Contributing centers provided for the vast majority disease classification as per WHO 2008. Pathology review was performed uniformly on the entire cohort, to ensure concordance between disease classification and diagnostic variables, and to update the classification as per WHO 2016. The cohort was representative of all MDS WHO subtypes and included 563 (17%) MDS/MPN and 167 (5%) AML/AML with myelodysplasia-related changes (AML-MRC) samples (Extended Data Table 1).

IPSS-R risk scores

IPSS-R risk scores were uniformly calculated based on the IPSS-R cytogenetic risk scores and on the values for hemoglobin, platelets, absolute neutrophil count and percentage of bone marrow blasts. All IPSS-R risk groups were represented (Extended Data Table 1).

Targeted sequencing

Panel design

The panel used for targeted sequencing included genes recurrently mutated in MDS as well as 1,118 genome wide single nucleotide polymorphism (SNP) probes for copy number analysis, with on average one SNP probe every 3Mb. Bait tiling was conducted at 2x. Baits were designed to span all exonic regions of *TP53* across all transcripts, as described in RefSeq (NM_001276761, NM_001276695, NM_001126114, NM_00112611), and included 20bp intronic flanking regions.

Library preparation and sequencing

For library construction, 11-800ng of genomic DNA was used using the KAPA Hyper Prep Kit (Kapa Biosystems KK8504) with 7-12 cycles of PCR. After sample barcoding, 10-1610ng of each library were pooled and captured by hybridization. Captured pools were sequenced with paired-end Illumina HiSeq at a median coverage of 730x per sample (range 127-2480x). Read length was 100bp or 125bp.

We also sequenced 48 samples on the panel, with the same sequencing conditions as the tumor samples, from young individuals who did not have hematological disease; to help further filtering of sequencing artefacts and germline SNPs.

Sequencing was performed in an unmatched setting i.e., without a matched normal tissue control per patient, so that variants had to be curated accordingly (see section "Variant calling and filtering for artefacts and likely germline variants" below).

Alignment

Raw sequence data were aligned to the human genome (NCBI build 37) using BWA[34] version 0.7.17. PCR duplicate reads were marked with Picard tools (https://broadinstitute.github.io/picard/) version 2.18.2. For alignment, we used the pcap-core dockerized pipeline version 4.2.1 available at https://github.com/cancerit/PCAP-core/wiki/Scripts-Reference-implementations.

Sample quality control

Quality control (QC) of the fastq data and bam data were performed with FastQC (http://www.bioinformatics.babraham.ac.uk/projects/fastqc/) version 0.11.5 and Picard tools respectively.

In addition, a number of downstream QC steps were performed, to include:

- Fingerprinting, i.e., evaluation of the similarity between all pairs of samples based on the respective genotype on 1,118 SNPs. Duplicate samples were excluded from the study.
- Evaluation of concordance between the patient sex from the clinical data and the coverage on the sex chromosomes. Discordant cases were discussed with the contributing centers to rule out patients with Klinefelter syndrome and filter out erroneous samples appropriately.
- Evaluation of concordance between CBA data and NGS derived copy-number profiles (see section "Copy number and LOH analysis" below). A typical discordant case is a case where CBA reports a given deletion or gain in a high number of metaphases and the NGS profile

clearly shows other abnormalities but not the one reported by CBA. All discordant cases were reviewed by a panel of experts through the IWG cytogenetic committee.

Finally, samples that passed QC but were found not to be treatment naive i.e., the patients received disease modifying treatment before sample collection were excluded from the study. Supplementary Fig. 1 summarizes the QC workflow.

Variant calling and filtering for artefacts and likely germline variants

Variants were called using a combination of variant callers. For single nucleotide variants (SNVs), we used Caveman (http://cancerit.github.io/CaVEMan/) version 1.7.4, Mutect[35] version 4.0.1.2 and Strelka[36] version 2.9.1. For small insertions and deletions (indels), we used Pindel[37] version 1.5.4, Mutect version 4.0.1.2 and Strelka version 2.9.1. VAFs were uniformly reported across all called variants using a "vafCorrect" realignment procedure available at https://github.com/cancerit/vafCorrect. All called variants were annotated with VAGrENT (https://github.com/cancerit/VAGrENT) version 3.3.0 and Ensembl-VEP (https://github.com/Ensembl/ensembl-vep) with Ensembl version 91 and VEP release 94.5.

Likely artefact variants were filtered out based on:

- Off-target variants, i.e., variants called outside of the panel target regions were excluded.
- Variants with VAF<2%, less than 20 total reads or less than 5 mutant supporting reads were excluded.
- The number of callers calling a given variant and the combination of filters (flags) from the triple callers. More specifically:
    - ➢ For SNVs, variants called by Caveman with more than 2 Caveman flags (from the DTH, RP, MN, PT, MQ, SR, TI, SRP, VUM, SE list) were excluded. Variants only called by Strelka and Mutect (not Caveman) were filtered out if they had >0 flags or if the "dirprop" metric (ratio of number of reads on each strand) was smaller than 0.44. Variants only called by Mutect (not Caveman nor Strelka) were filtered out if they had >0 flags or if "dirprop" was smaller than 0.44 or if VAF was smaller than 5%.
    - ➢ For indels, variants called by all three callers Pindel, Mutect and Strelka were excluded if they had >3 flags. Variants called by only two callers were excluded if

they had >2 flags. Variants only called by Pindel were filtered out if they had >1 flags or less than 2 mutant reads on one strand. Variants only called by Mutect were filtered out if they had >0 flags or less than 2 mutant reads on one strand.

- Recurrence and VAF distribution of the called variants on a panel of 48 normals samples.

After pre-filtering of artifactual variants, likely germline SNPs were filtered out by consideration of:

- VAF density of variants consistent with germline SNP.
- Presence in the Genome Aggregation Database (gnomAD)[38]. More specifically, variants with a population based allele frequency ("VEP_gnomAD_AF") larger than 0.001 were excluded (with the exception of a few variants in *SH2B3* involved in familial thrombocythemia). Variants with a maximum allele frequency across the gnomAD populations ("VEP_MAX_AF") larger than 0.01 were excluded (with the exception of *ASXL1* amino acid position G646 which requires specific rescue).
- Recurrence in panel of normals.

All remaining likely somatic variants after abovementioned filtering were manually inspected with the Integrative Genomics Viewer (IGV)[39] to rule out residual artefacts.

Variant annotation for likely oncogenicity

From the list of likely somatic variants, putative oncogenic variants were distinguished from variants of unknown significance VUS based on:

- Recurrence in the Catalogue Of Somatic Mutations in Cancer (COSMIC)[40], in myeloid disease samples registered in cBioPortal[40,41] or in the study dataset.
- Presence in pan-cancer hotspot databases[42,43].
- Annotation in the human variation database ClinVar[44].
- Annotation in the precision oncology knowledge database OncoKB[45].
- Recurrence with somatic presentation in a set of in-house data derived from >6,000 myeloid neoplasms[16,32,46].

- The inferred consequence of a mutation; where nonsense mutations, splice site mutations and frameshift indels were considered oncogenic for likely tumor suppressor genes (from COSMIC Cancer Census Genes or OncoKB Cancer Gene List).

For annotation of oncogenicity of *TP53* variants we additionally considered:

- Functional annotation in the International Agency for Research on Cancer (IARC) *TP53* database[47].
- Functional classification *TP53* prediction scores using PHANTM[48].

Supplementary Figure 5 illustrates the rational and results of the annotation of variants for putative oncogenicity.

Copy number and LOH analysis

In addition to CBA, we assessed chromosomal alterations based on NGS sequencing data using CNACS[7]. CNACS enables the detection of arm level and focal copy-numbers changes as well as regions of cnLOH. CNACS has been optimized to run in the unmatch setting and uses a panel of normals for calibration.

Supplementary Fig. 2 provides examples of characterization of allelic imbalances (gains, deletions and regions of cnLOH) using CNACS, with concordant copy-number change findings between CBA and CNACS, focal deletions exclusively detected with CNACS and, as expected, regions of cnLOH detected by CNACS only. For genome-wide analysis, we restricted the CNACS segments to be bigger than 3Mb with a minor-allele-frequency smaller than 45% (when 50% represents no allelic imbalance). Supplementary Fig. 4 provides examples of characterization of allelic imbalances by CNACS and SNP arrays on 21 selected samples, with very concordant findings between the two assays.

In addition to CNACS, we also run CNVkit[49] version 0.9.6 on the study cohort. CNVkit does not infer allele specific copy-numbers, so that it does not allow to mark regions of cnLOH, but it estimates copy-number changes. The integration of two copy-number tools increased specificity and sensitivity of the copy-number calling.

On 2,931 patients with CBA data, we performed a detailed comparison of CBA and NGS-derived copy-number results (Supplementary Fig. 3) and showed highly concordant findings. Along with the annotation of regions of cnLOH, we supplemented the presence of copy-number changes on patients when it was clear on the NGS results but missed by CBA (e.g. focal deletions). In 393 patients with missing CBA data, we used the NGS results to fully annotate copy-number changes. As our NGS assay did not allow to detect translocations, inversions, whole genome amplification and the presence of marker or ring chromosomes, those specific alterations were statistically imputed from other molecular markers on these 393 patients.

Complex Karyotype

From the 2,931 patients with CBA data, 310 had a complex karyotype according to the CBA results, where complex karyotype was defined as 3 or more independent chromosomal abnormalities. Within the 2,931 patients with CBA data, NGS results helped to identify complex karyotypes in an additional 15 patients. Within the 393 cases with missing CBA data, 13 had a complex karyotype according to NGS copy-number profiles (Supplementary Fig. 3c). Overall, 329 patients had a complex karyotype representing 10% of the study cohort.

Survival analysis

All statistical analyses were conducted using the R statistical platform (R Core Team 2019) (https://www.r-project.org/). Kaplan-Meir estimates were computed using the "survival" package and estimates of AML transformation from the "cmprsk" package. Cox proportional hazards regressions were performed using the "coxph" package.

Overall survival

OS was measured from the time of sample collection to the time of death from any cause. Patients alive at the last follow-up date were censored at that time. Survival probabilities over time were estimated using Kaplan-Meier methodology, and comparisons of survival across *TP53*-mutant subgroups were conducted using the logrank test.

Multivariable models of OS were performed with Cox proportional hazards regressions. Hazard ratios and 95% confidence intervals were reported for the covariates along the p-values from the

Wald test. Covariates included in the multivariable model of OS were age, hemoglobin, platelets, absolute neutrophil count (ANC), bone marrow blasts, cytogenetic risk group and *TP53* allelic state. Hemoglobin, platelets, ANC and bone marrow blasts were treated as continuous variables and were scaled by their sample mean. Age was treated as a continuous variable and was scaled by a factor 10. Cytogenetic risk group was treated as a categorical variable with the intermediate risk group as the reference group. *TP53* allelic state was treated as a categorical variable with the wild-type state as the reference group relative to the mono-allelic and the multi-hit groups. Those covariates correspond to all covariates included in the age-adjusted IPPS-R model along the *TP53* allelic state.

AML transformation

In univariate analysis of AML transformation (AMLt), time to AMLt was measured from the time of sample collection to the time of transformation, with death without transformation treated as a competing risk. Patients alive without AMLt at the last contact date were censored at that time. Cumulative incidence functions were used to estimate the incidence of AMLt and comparisons of cumulative incidence function across *TP53*-mutant subgroups were conducted using Gray's test.

Multivariable models of AMLt were performed using cause-specific Cox proportional hazards regressions, where patients who did not transform but died were censored at the time of death. Hazard ratios and 95% confidence intervals were reported for the covariates along the p-values from the Wald test. Covariates included in the multivariable model of AMLt were the same as the ones included in the model of OS described above.

Data accessibility

Clinical, copy-number and *TP53* mutation data are available on Github, see the data folder of https://github.com/papaemmelab/MDS-TP53-state. The list of SNPs included in the custom capture next generation sequencing panel is also available.

Code reproducibility

The NGS-based allele specific copy-number algorithm CNACS[7] is available as a python toil workflow engine at https://github.com/papaemmelab/toil_cnacs, where release v0.2.0 was used in this study.

Results and figures from the manuscript can be reproduced by running the code documented and available as a jupyter notebook or an html file at https://github.com/papaemmelab/MDS-TP53-state.

AUTHOR CONTRIBUTIONS

E.B. and E.P. designed the study. E.B. and Y.N. performed statistical analysis. S.D. and E.P. supervised statistical analysis. L.M., B.L.E, R.B., P.L.G., M. Cazzola, E.H-L., S.O. and E.P. supervised research. P.L.G. and E.P. coordinated the study. L.M., F.S., C.A.C., M. Creignou, U.G., A.A.L., M.J., M.T., O.K., M.Y.F., F.T., R.F.P., V.S., I.K., J.B., F.P.S.S., S.K., T.I., T.H., A.K.T., T.K., C.P., V.M.K., M.R.S., M.B., C.G., L.P., L.A., M.G.D.P., P.F., A.P., U.P., M.H., P.V., S.C., Y.M., C.F., M.T.V., L-Y.S., M.F., J.H.J., J.C., Y.A., N.G., M. Cazzola, E.H-L. and S.O. provided clinical data and DNA specimens. E.B., Y.W., M.P. and E.P. coordinated sample acquisition. A.V. and K.V. performed sample preparation and sequencing. E.B., R.P.H., H.T. and M. Creignou curated clinical data. R.P.H. and J.M.B. performed pathology review. E.B. and H.T. processed cytogenetic data. F.S., D.H. and J.S. performed cytogenetic review. E.B., Y.N., J.S.M-M, T.Y., A.S. and G.G. performed bioinformatic analysis. J.S.M-M, M.F.L., J.E.A. and J.Z. supported sequence data pipelines. Y.S. and R.S. developed copy-number algorithm CNACS. M.F.L. generated copy-number profiles. Y.Z. performed SNP array analysis. E.B. and Y.N. prepared figures and tables. E.B., S.O. and E.P. wrote the manuscript. All authors reviewed the manuscript during its preparation.

ACKNOWLEDGEMENTS

Supported in part by grants from Celgene Corporation through and MDS Foundation, Inc, Yardville, NJ; J.B. and A.P. acknowledge funding from Bloodwise grant 13042; P.V. was supported by the Austrian Science Fund (FWF) grant F4704-B20; M.Y.F. was supported by Italian

MIUR-PRIN grants; L.M. was supported by the Associazione Italiana per la Ricerca sul Cancro (AIRC, Milan, Italy) 5×1000 project #21267 and IG #20125; M.T.V. was supported by AIRC 5 per Mille project #21267 and patients were recruited through the GROM-L clinical network; E.B. was supported by the Francois Wallace Monahan Fellowship; E.P. is a Josie Robertson Investigator and is supported by the European Hematology Association, American Society of Hematology, Gabrielle's Angels Foundation, V Foundation and The Geoffrey Beene Foundation. We thank Tracey Iraca for logistic support.

REFERENCES

1. Kandoth, C. *et al.* Mutational landscape and significance across 12 major cancer types. *Nature* **502**, 333–339 (2013).
2. Zehir, A. *et al.* Mutational landscape of metastatic cancer revealed from prospective clinical sequencing of 10,000 patients. *Nat. Med.* **23**, 703–713 (2017).
3. Haase, D. *et al.* TP53 mutation status divides myelodysplastic syndromes with complex karyotypes into distinct prognostic subgroups. *Leukemia* vol. 33 1747–1758 (2019).
4. Bejar, R. *et al.* Clinical effect of point mutations in myelodysplastic syndromes. *N. Engl. J. Med.* **364**, 2496–2506 (2011).
5. Kitagawa, M., Yoshida, S., Kuwata, T., Tanizawa, T. & Kamiyama, R. p53 expression in myeloid cells of myelodysplastic syndromes. Association with evolution of overt leukemia. *Am. J. Pathol.* **145**, 338–344 (1994).
6. Lindsley, R. C. *et al.* Prognostic Mutations in Myelodysplastic Syndrome after Stem-Cell Transplantation. *N. Engl. J. Med.* **376**, 536–547 (2017).
7. Yoshizato, T. *et al.* Genetic abnormalities in myelodysplasia and secondary acute myeloid leukemia: impact on outcome of stem cell transplantation. *Blood* **129**, 2347–2358 (2017).

8. Jädersten, M. *et al.* TP53 mutations in low-risk myelodysplastic syndromes with del(5q) predict disease progression. *J. Clin. Oncol.* **29**, 1971–1979 (2011).
9. Haferlach, T. *et al.* Landscape of genetic lesions in 944 patients with myelodysplastic syndromes. *Leukemia* **28**, 241–247 (2014).
10. Kastenhuber, E. R. & Lowe, S. W. Putting p53 in Context. *Cell* **170**, 1062–1078 (2017).
11. Greenberg, P. L. *et al.* Revised international prognostic scoring system for myelodysplastic syndromes. *Blood* **120**, 2454–2465 (2012).
12. Schanz, J. *et al.* New comprehensive cytogenetic scoring system for primary myelodysplastic syndromes (MDS) and oligoblastic acute myeloid leukemia after MDS derived from an international database merge. *J. Clin. Oncol.* **30**, 820–829 (2012).
13. Breems, D. A. *et al.* Monosomal karyotype in acute myeloid leukemia: a better indicator of poor prognosis than a complex karyotype. *J. Clin. Oncol.* **26**, 4791–4797 (2008).
14. Donehower, L. A. *et al.* Integrated Analysis of TP53 Gene and Pathway Alterations in The Cancer Genome Atlas. *Cell Rep.* **28**, 3010 (2019).
15. Rucker, F. G. *et al.* TP53 alterations in acute myeloid leukemia with complex karyotype correlate with specific copy number alterations, monosomal karyotype, and dismal outcome. *Blood* vol. 119 2114–2121 (2012).
16. Papaemmanuil, E. *et al.* Genomic Classification and Prognosis in Acute Myeloid Leukemia. *N. Engl. J. Med.* **374**, 2209–2221 (2016).
17. Sallman, D. A. *et al.* Impact of TP53 mutation variant allele frequency on phenotype and outcomes in myelodysplastic syndromes. *Leukemia* **30**, 666–673 (2016).
18. Goel, S. *et al.* High prevalence and allele burden-independent prognostic importance of p53 mutations in an inner-city MDS/AML cohort. *Leukemia* vol. 30 1793–1795 (2016).

19. Montalban-Bravo, G. *et al.* Genomic context and TP53 allele frequency define clinical outcomes in TP53-mutated myelodysplastic syndromes. *Blood Adv* **4**, 482–495 (2020).
20. Lausen, B. & Schumacher, M. Maximally Selected Rank Statistics. *Biometrics* vol. 48 73 (1992).
21. Boettcher, S. *et al.* A dominant-negative effect drives selection of TP53 missense mutations in myeloid malignancies. *Science* vol. 365 599–604 (2019).
22. Levine, A. J. The many faces of p53: something for everyone. *J. Mol. Cell Biol.* (2019) doi:10.1093/jmcb/mjz026.
23. Lang, G. A. *et al.* Gain of Function of a p53 Hot Spot Mutation in a Mouse Model of Li-Fraumeni Syndrome. *Cell* vol. 119 861–872 (2004).
24. Olive, K. P. *et al.* Mutant p53 Gain of Function in Two Mouse Models of Li-Fraumeni Syndrome. *Cell* vol. 119 847–860 (2004).
25. Loizou, E. *et al.* A Gain-of-Function p53-Mutant Oncogene Promotes Cell Fate Plasticity and Myeloid Leukemia through the Pluripotency Factor FOXH1. *Cancer Discov.* **9**, 962–979 (2019).
26. Wong, T. N. *et al.* Role of TP53 mutations in the origin and evolution of therapy-related acute myeloid leukaemia. *Nature* **518**, 552–555 (2015).
27. Platzbecker, U. Treatment of MDS. *Blood* **133**, 1096–1107 (2019).
28. Roman, E. *et al.* Myeloid malignancies in the real-world: Occurrence, progression and survival in the UK's population-based Haematological Malignancy Research Network 2004–15. *Cancer Epidemiology* vol. 42 186–198 (2016).
29. Smith, A. *et al.* Cohort Profile: The Haematological Malignancy Research Network (HMRN); a UK population-based patient cohort. *Int. J. Epidemiol.* (2018) doi:10.1093/ije/dyy044.

30. Welch, J. S. *et al.* TP53 and Decitabine in Acute Myeloid Leukemia and Myelodysplastic Syndromes. *N. Engl. J. Med.* **375**, 2023–2036 (2016).
31. Malcovati, L. *et al.* Clinical significance of SF3B1 mutations in myelodysplastic syndromes and myelodysplastic/myeloproliferative neoplasms. *Blood* **118**, 6239–6246 (2011).
32. Papaemmanuil, E. *et al.* Clinical and biological implications of driver mutations in myelodysplastic syndromes. *Blood* **122**, 3616–27; quiz 3699 (2013).
33. International Standing Committee on Human Cytogenetic Nomenclature. *ISCN 2013: An International System for Human Cytogenetic Nomenclature (2013)*. (Karger Medical and Scientific Publishers, 2013).
34. Li, H. & Durbin, R. Fast and accurate long-read alignment with Burrows-Wheeler transform. *Bioinformatics* **26**, 589–595 (2010).
35. Cibulskis, K. *et al.* Sensitive detection of somatic point mutations in impure and heterogeneous cancer samples. *Nat. Biotechnol.* **31**, 213–219 (2013).
36. Saunders, C. T. *et al.* Strelka: accurate somatic small-variant calling from sequenced tumor-normal sample pairs. *Bioinformatics* **28**, 1811–1817 (2012).
37. Ye, K., Schulz, M. H., Long, Q., Apweiler, R. & Ning, Z. Pindel: a pattern growth approach to detect break points of large deletions and medium sized insertions from paired-end short reads. *Bioinformatics* **25**, 2865–2871 (2009).
38. Karczewski, K. J. *et al.* Variation across 141,456 human exomes and genomes reveals the spectrum of loss-of-function intolerance across human protein-coding genes. doi:10.1101/531210.
39. Thorvaldsdóttir, H., Robinson, J. T. & Mesirov, J. P. Integrative Genomics Viewer (IGV): high-performance genomics data visualization and exploration. *Brief. Bioinform.* **14**,

178–192 (2013).

40. Tate, J. G. *et al.* COSMIC: the Catalogue Of Somatic Mutations In Cancer. *Nucleic Acids Res.* **47**, D941–D947 (2019).
41. Cerami, E. *et al.* The cBio cancer genomics portal: an open platform for exploring multidimensional cancer genomics data. *Cancer Discov.* **2**, 401–404 (2012).
42. Chang, M. T. *et al.* Identifying recurrent mutations in cancer reveals widespread lineage diversity and mutational specificity. *Nat. Biotechnol.* **34**, 155–163 (2016).
43. Chang, M. T. *et al.* Accelerating Discovery of Functional Mutant Alleles in Cancer. *Cancer Discov.* **8**, 174–183 (2018).
44. Landrum, M. J. *et al.* ClinVar: public archive of relationships among sequence variation and human phenotype. *Nucleic Acids Res.* **42**, D980–5 (2014).
45. Chakravarty, D. *et al.* OncoKB: A Precision Oncology Knowledge Base. *JCO Precis Oncol* **2017**, (2017).
46. Grinfeld, J. *et al.* Classification and Personalized Prognosis in Myeloproliferative Neoplasms. *N. Engl. J. Med.* **379**, 1416–1430 (2018).
47. Bouaoun, L. *et al.* TP53 Variations in Human Cancers: New Lessons from the IARC TP53 Database and Genomics Data. *Hum. Mutat.* **37**, 865–876 (2016).
48. Giacomelli, A. O. *et al.* Mutational processes shape the landscape of TP53 mutations in human cancer. *Nat. Genet.* **50**, 1381–1387 (2018).
49. Talevich, E., Shain, A. H., Botton, T. & Bastian, B. C. CNVkit: Genome-Wide Copy Number Detection and Visualization from Targeted DNA Sequencing. *PLoS Comput. Biol.* **12**, e1004873 (2016).

FIGURES AND EXTENDED DATA LEGENDS

Figure 1 | Integration of *TP53* mutations and allelic imbalances at the *TP53* locus identifies *TP53* states with evidence of mono-allelic or bi-allelic targeting.

Figure 2 | *TP53* allelic state correlates with contrasting levels of genome stability and patterns of co-mutation.

Figure 3 | *TP53* allelic state associates with distinct clinical phenotypes and shapes patient outcomes.

Figure 4 | *TP53* allelic state demarcates outcomes in therapy-related MDS and on different therapies.

Extended Data Figure 1 | Landscape of chromosomal aberrations in MDS.

Extended Data Figure 2 | Evidence of bi-allelic *TP53* targeting in the cases with multiple *TP53* mutations.

Extended Data Figure 3 | Heatmap of chromosomal aberrations per *TP53* allelic state.

Extended Data Figure 4 | *TP53* allelic state segregates patient outcomes across WHO subtypes and IPSS-R risk groups.

Extended Data Figure 5 | Outcomes across *TP53* subgroups and VAF strata.

Extended Data Figure 6 | Maintained differences in genome instability levels and outcomes per *TP53* state across mutation types.

Extended Data Figure 7 | Clinical workflow for the assessment of *TP53* allelic state.

Extended Data Table 1 | Study cohort characteristics.

Extended Data Table 2 | Validation cohort characteristics.

Extended Data Table 3 | Characteristics of treated cohort subsets.

Figure 1 | Integration of *TP53* mutations and allelic imbalances at the *TP53* locus identifies *TP53* states with evidence of mono-allelic or bi-allelic targeting. a, Number of patients (from patients with any hit at the *TP53* locus) with 0, 1, 2 or 3 *TP53* mutations. Colors represent the status of chromosome 17 at the *TP53* locus, to include copy-neutral loss of heterozygosity (cnloh), deletion (del), isochromosome 17q rearrangement (iso17q), gain or no detected aberration (normal). Unbalanced translocations leading to 17p deletion are encoded as "del". **b,** Frequency of *TP53* subgroups within *TP53*-mutated patients. *TP53* subgroups are defined as cases with i) single gene mutation (1mut) ii) several mutations with normal status of chromosome 17 at the *TP53* locus (>1mut) iii) mutation(s) and chromosomal deletion at the *TP53* locus (mut+del) and iv) mutation(s) and copy-neutral loss of heterozygosity at the *TP53* locus (mut+cnloh). **c,** Density estimation of variant allele frequency (VAF) of *TP53* mutations across *TP53* subgroups (1mut, >1mut, mut+del, mut+cnloh from top to bottom). **d,** Distribution of *TP53* mutations along the gene body. Mutations from patients with mono-allelic *TP53* are depicted at the top and mutations from patients with multiple *TP53* hits at the bottom. Missense mutations are shown as green circles. Truncated mutations corresponding to nonsense or nonstop mutations, frameshift deletions or insertions and splice site variants are shown as pink circles. Other types of mutations to include inframe deletions or insertions are shown as orange circles. TAD: transactivation domain; DBD: DNA binding domain; OD: oligomerization domain.

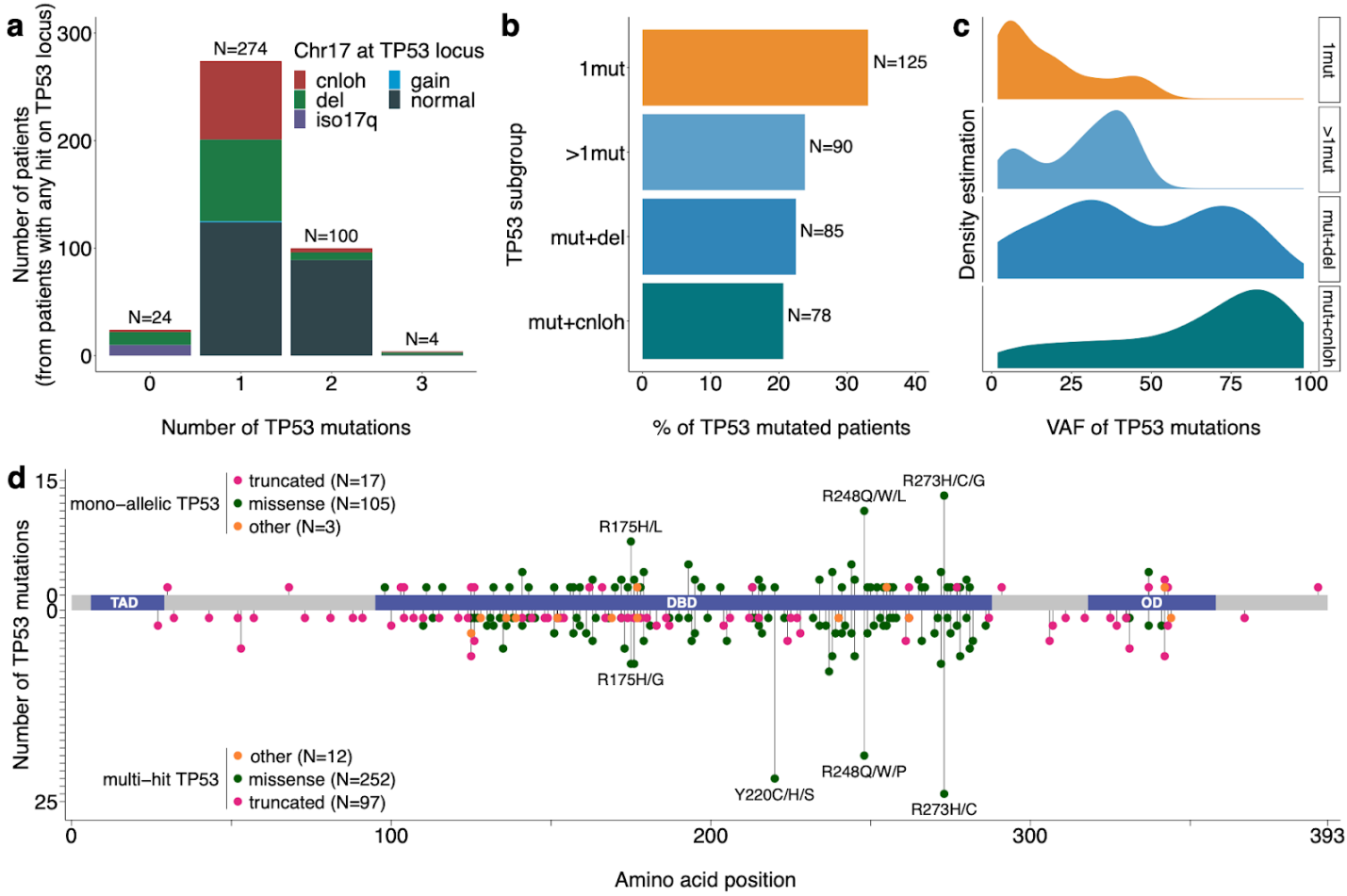
a
Number of patients
(from patients with any hit on TP53 locus)
300
200
100
0
N=24
N=274
N=100
N=4
Chr17 at TP53 locus
cnloh
del
iso17q
gain
normal
0
1
2
3
Number of TP53 mutations
b
TP53 subgroup
1mut
>1mut
mut+del
mut+cnloh
N=125
N=90
N=85
N=78
0
10
20
30
40
% of TP53 mutated patients
c
Density estimation
1mut
>1mut
mut+del
mut+cnloh
0
25
50
75
100
VAF of TP53 mutations
d
Number of TP53 mutations
15
0
0
25
mono−allelic TP53
truncated (N=17)
missense (N=105)
other (N=3)
multi−hit TP53
other (N=12)
missense (N=252)
truncated (N=97)
TAD
DBD
OD
R175H/L
R175H/G
R248Q/W/L
R273H/C/G
Y220C/H/S
R248Q/W/P
R273H/C
0
100
200
300
393
Amino acid position

Figure 2 | *TP53* allelic state correlates with contrasting levels of genome stability and patterns of co-mutation. a, Distribution of the number of chromosomal aberrations on other chromosomes than 17 per patient across *TP53* subgroups and types of aberrations, i.e., rearrangement (rearr), gain or deletion (del). Boxplot centres, hinges and whiskers represent the median, first and third quartiles and 1.5 x interquartile range, respectively. ****p<0.0001, Wilcoxon rank-sum test, each compared to the same aberration within the 1mut group. **b,** Number of unique chromosomes other than 17 affected by a chromosomal aberration (rearrangement, deletion or gain) per *TP53* subgroup. Dots represent the median across patients and lines extend from first to third quartiles. ****p<0.0001, Wilcoxon rank-sum test, compared to the 1mut group. **c,** Interaction between *TP53* allelic state and complex karyotype. 13% (16/125) of mono-allelic *TP53* patients (1mut) had a complex karyotype and 91% (231/253) of multi-hit *TP53* patients (multi) had a complex karyotype. **d,** Number of driver mutations on other genes than *TP53* per *TP53* subgroup. **e,** Proportion of cases per *TP53* allelic state with driver mutations in the genes most frequently co-mutated with *TP53*. Genes mutated in at least 5% of mono-allelic or multi-hit patients are represented. *p<0.05, **p<0.01, ***p<0.001, Fisher exact test with Benjamini-Hochberg multiple testing correction.

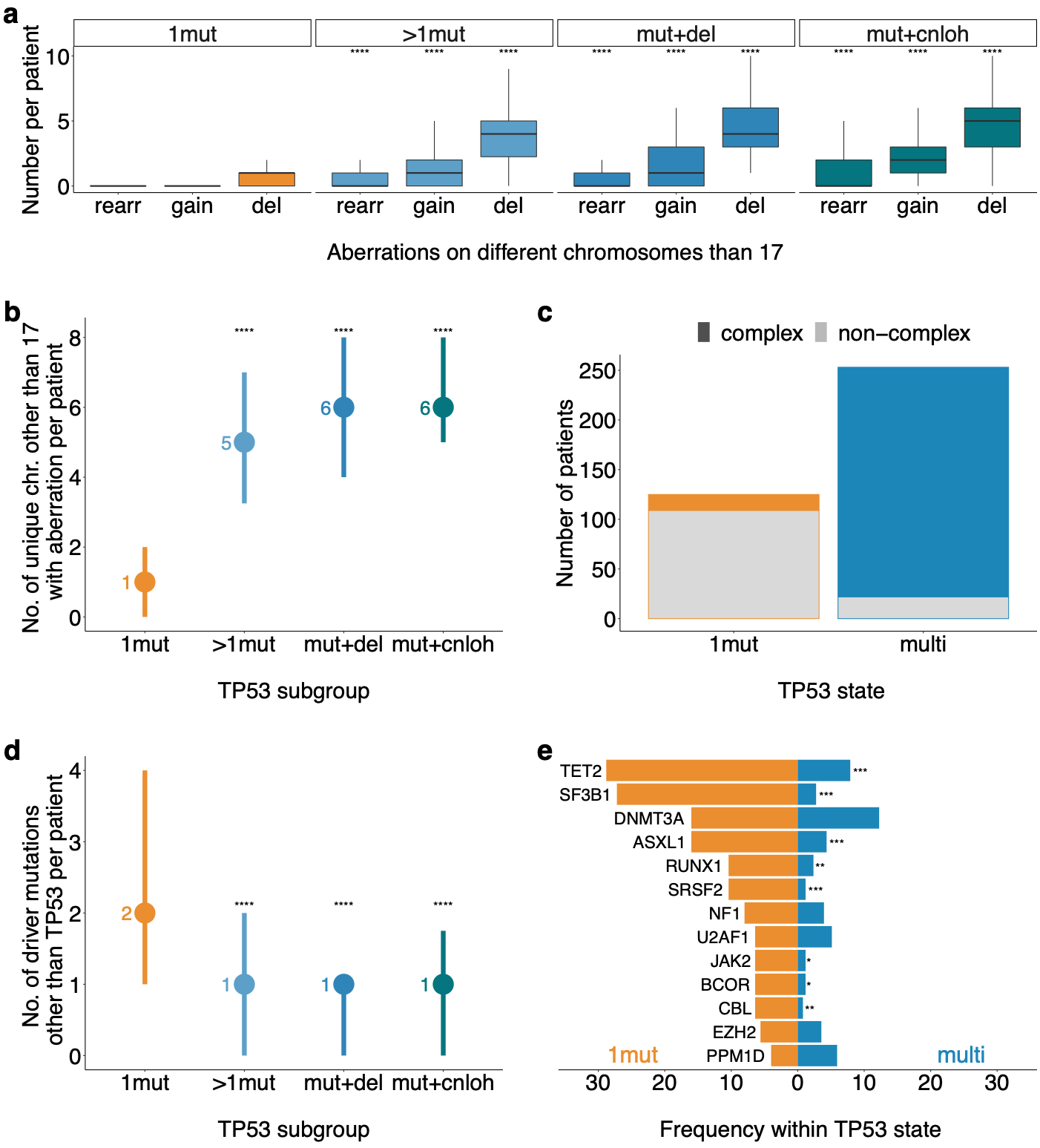
a
1mut
>1mut
mut+del
mut+cnloh
Number per patient
rearr
gain
del
Aberrations on different chromosomes than 17
b
No. of unique chr. other than 17 with aberration per patient
1mut
>1mut
mut+del
mut+cnloh
TP53 subgroup
c
complex
non−complex
Number of patients
1mut
multi
TP53 state
d
No. of driver mutations other than TP53 per patient
TP53 subgroup
e
TET2
SF3B1
DNMT3A
ASXL1
RUNX1
SRSF2
NF1
U2AF1
JAK2
BCOR
CBL
EZH2
PPM1D
1mut
multi
Frequency within TP53 state

Figure 3 | *TP53* allelic state associates with distinct clinical phenotypes and shapes patient outcomes. a-c, Boxplots indicative of the levels of cytopenias per *TP53* allelic state of wild-type *TP53* (WT), mono-allelic *TP53* (1mut) or multiple *TP53* hits (multi), respectively hemoglobin in (a), platelets in (b) and absolute neutrophil count (ANC) in (c). **d,** Percentage of bone marrow blasts per *TP53* allelic state. Boxplot centres, hinges and whiskers represent the median, first and third quartiles and 1.5 x interquartile range, respectively. The y-axes are square-rooted. ***p<0.001, ****p<0.0001, Wilcoxon rank-sum test. **e-f,** Kaplan-Meier probability estimates of overall survival (e) and cumulative incidence of AML transformation (AMLt) (f) per *TP53* allelic state. **g,** Results of Cox proportional hazards regression for overall survival (OS) performed on 2,719 patients with complete data for OS and with 1,290 observed death. Explicative variables are hemoglobin, platelets, ANC, bone marrow blasts, cytogenetic IPSS-R risk scores (very-good, good, intermediate is the reference, poor and very-poor) and *TP53* allelic state (mono-allelic, multi-hit and wild-type is the reference). Hemoglobin, platelets, ANC and bone marrow blasts are scaled by their sample mean. Age is scaled by a factor 10. The x-axis is $\log_{10}$ scaled. **h,** Results of cause-specific Cox proportional hazards regression for AMLt performed on 2,464 patients with complete data for AMLt and with 411 observed transformation. Covariates are the same as in (g). ****p<0.0001, ***p<0.001, **p<0.01, *p<0.05 Wald test.

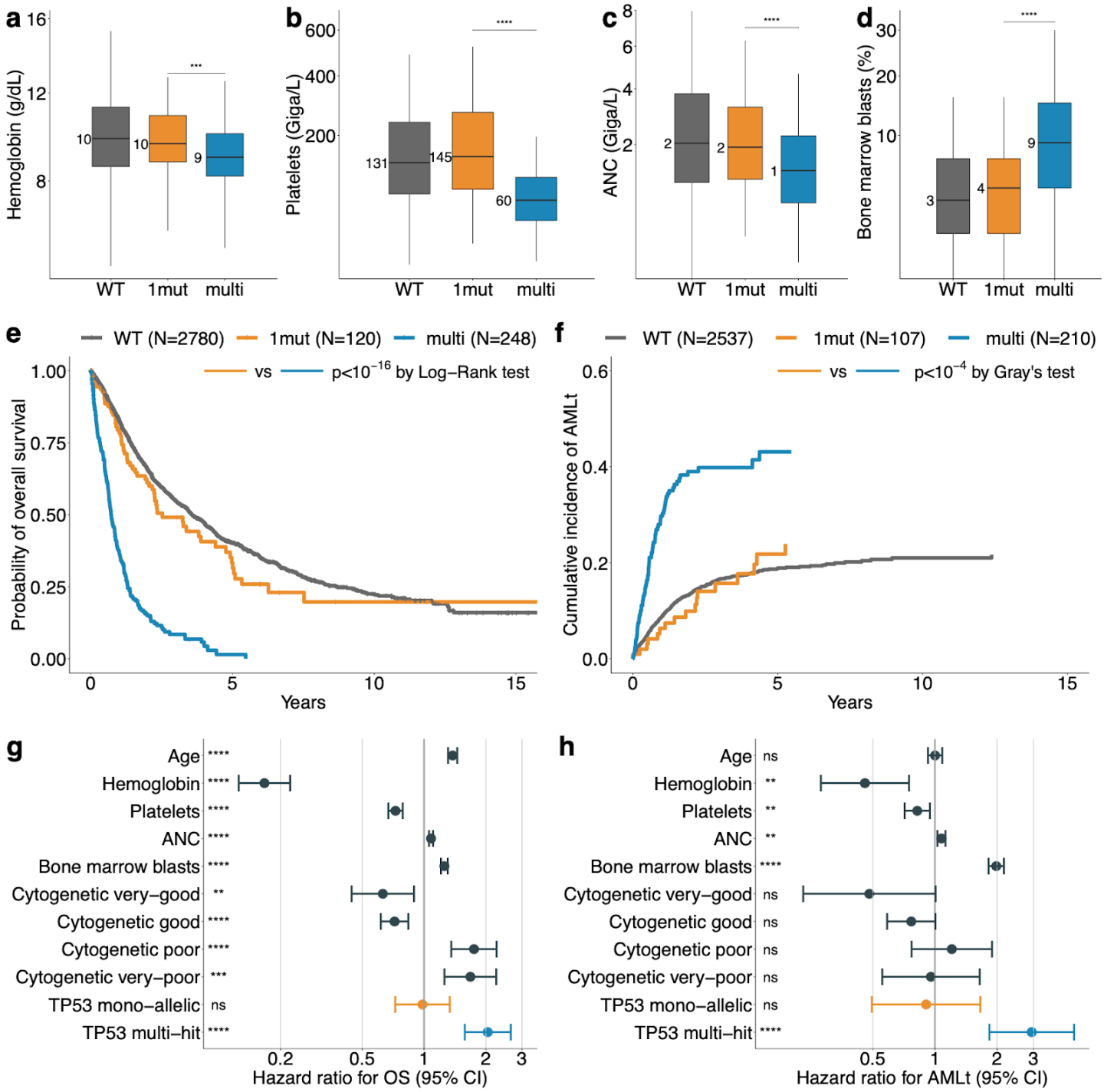
a
Hemoglobin (g/dL)
16
12
8
***
10
10
9
WT
1mut
multi
b
Platelets (Giga/L)
600
400
200
****
131
145
60
WT
1mut
multi
c
ANC (Giga/L)
8
6
4
2
****
2
2
1
WT
1mut
multi
d
Bone marrow blasts (%)
30
20
10
****
3
4
9
WT
1mut
multi
e
WT (N=2780)
1mut (N=120)
multi (N=248)
vs
p<10−16 by Log−Rank test
Probability of overall survival
1.00
0.75
0.50
0.25
0.00
0
5
10
15
Years
f
WT (N=2537)
1mut (N=107)
multi (N=210)
vs
p<10−4 by Gray's test
Cumulative incidence of AMLt
0.6
0.4
0.2
0.0
0
5
10
15
Years
g
Age ****
Hemoglobin ****
Platelets ****
ANC ****
Bone marrow blasts ****
Cytogenetic very−good **
Cytogenetic good ****
Cytogenetic poor ****
Cytogenetic very−poor ***
TP53 mono−allelic ns
TP53 multi−hit ****
0.2
0.5
1
2
3
Hazard ratio for OS (95% CI)
h
Age ns
Hemoglobin **
Platelets **
ANC **
Bone marrow blasts ****
Cytogenetic very−good ns
Cytogenetic good ns
Cytogenetic poor ns
Cytogenetic very−poor ns
TP53 mono−allelic ns
TP53 multi−hit ****
0.5
1
2
3
Hazard ratio for AMLt (95% CI)

Figure 4 | *TP53* allelic state demarcates outcomes in therapy-related MDS and on different therapies. a, Kaplan-Meier probability estimates of overall survival per *TP53* allelic state of wild-type *TP53* (WT), mono-allelic *TP53* (1mut) and multiple *TP53* hits (multi); and across types of MDS, i.e., de-novo MDS (solid line) or therapy-related MDS (dashed line). Within the therapy-related cases, 10 had a mono-allelic *TP53* mutation (dashed orange line), 52 were multi-hit *TP53* (dashed blue line) and 162 were *TP53* wild-type (dashed grey line). **b-c-d**, Kaplan-Meier probability estimates of overall survival post start of hypomethylating agent (HMA) treatment **(b)** start of Lenalidomide treatment for patients with del(5q) **(c)** hematopoietic stem cell transplantation (HSCT) **(d)** per *TP53* allelic state. In (b), (c), and (d), overall survival was measured from the time of treatment start or HSCT to the time of death from any cause. Patients alive at the last follow-up date were censored at that time. Annotated p-values are from the log-rank test.

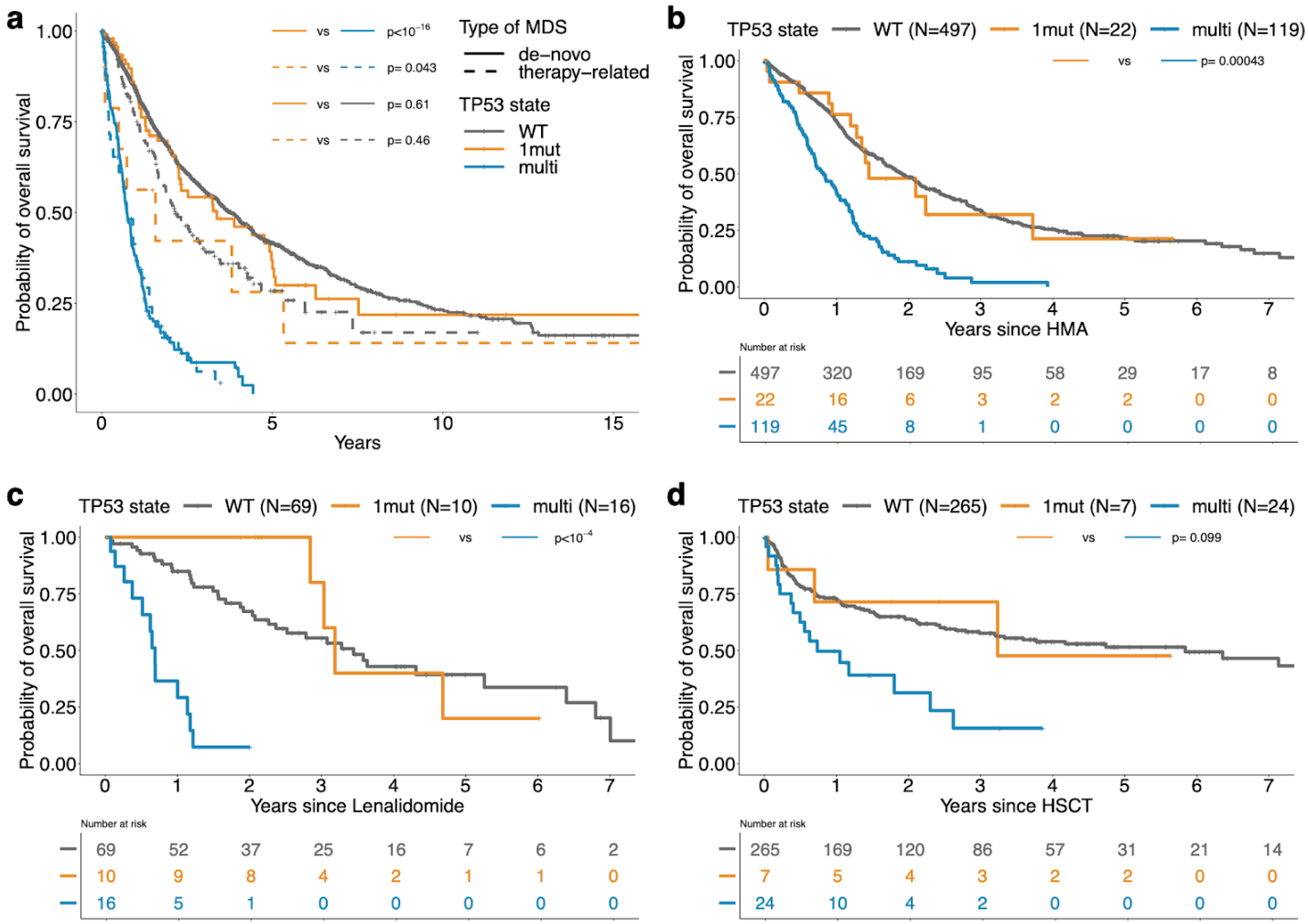
a
Probability of overall survival
1.00
0.75
0.50
0.25
0.00
0
5
10
15
Years
vs p<10^-16
vs p= 0.043
vs p= 0.61
vs p= 0.46
Type of MDS
de−novo
therapy−related
TP53 state
WT
1mut
multi
b
TP53 state WT (N=497) 1mut (N=22) multi (N=119)
vs p= 0.00043
Years since HMA
Number at risk
497 320 169 95 58 29 17 8
22 16 6 3 2 2 0 0
119 45 8 1 0 0 0 0
c
TP53 state WT (N=69) 1mut (N=10) multi (N=16)
vs p<10^-4
Years since Lenalidomide
Number at risk
69 52 37 25 16 7 6 2
10 9 8 4 2 1 1 0
16 5 1 0 0 0 0 0
d
TP53 state WT (N=265) 1mut (N=7) multi (N=24)
vs p= 0.099
Years since HSCT
Number at risk
265 169 120 86 57 31 21 14
7 5 4 3 2 2 0 0
24 10 4 2 0 0 0 0

Extended Data Figure 1 | Landscape of chromosomal aberrations in MDS. a. Landscape of chromosomal arm-level aberrations across 3,324 patients. Aberrations include copy-neutral loss-of-heterozygosity (cnloh), deletion (del) and gain. The x-axis indicates chromosome arms or entire chromosomes affected by aberrations. Aberrations were assessed using the integration of conventional G-banding analysis (CBA) data and NGS derived allele specific copy-number profiles (see Methods). NGS aberrant segments were restricted to segments larger than 3 megabases. **b.** Frequency distribution of chromosomal aberrations ordered by type of aberrations. First top three plots represent arm-level copy-neutral loss-of-heterozygosity (cnloh), deletion (del) and gain. Fourth bottom plot represents other types of aberrations to include the presence of marker chromosome (mar), rearrangements where r_i_j denotes a rearrangement between chromosome i and j, isochromosome 17q (iso17q), whole genome amplification (WGA) and presence of ring chromosome (ring). All aberrations observed in more than 2 patients are depicted. Of note, cnloh is detectable with NGS but not with CBA. On the opposite, rearrangements, presence of marker or ring chromosome and WGA were only assessed from CBA data. In 393 cases with missing CBA data, those specific aberrations were imputed from other molecular markers.

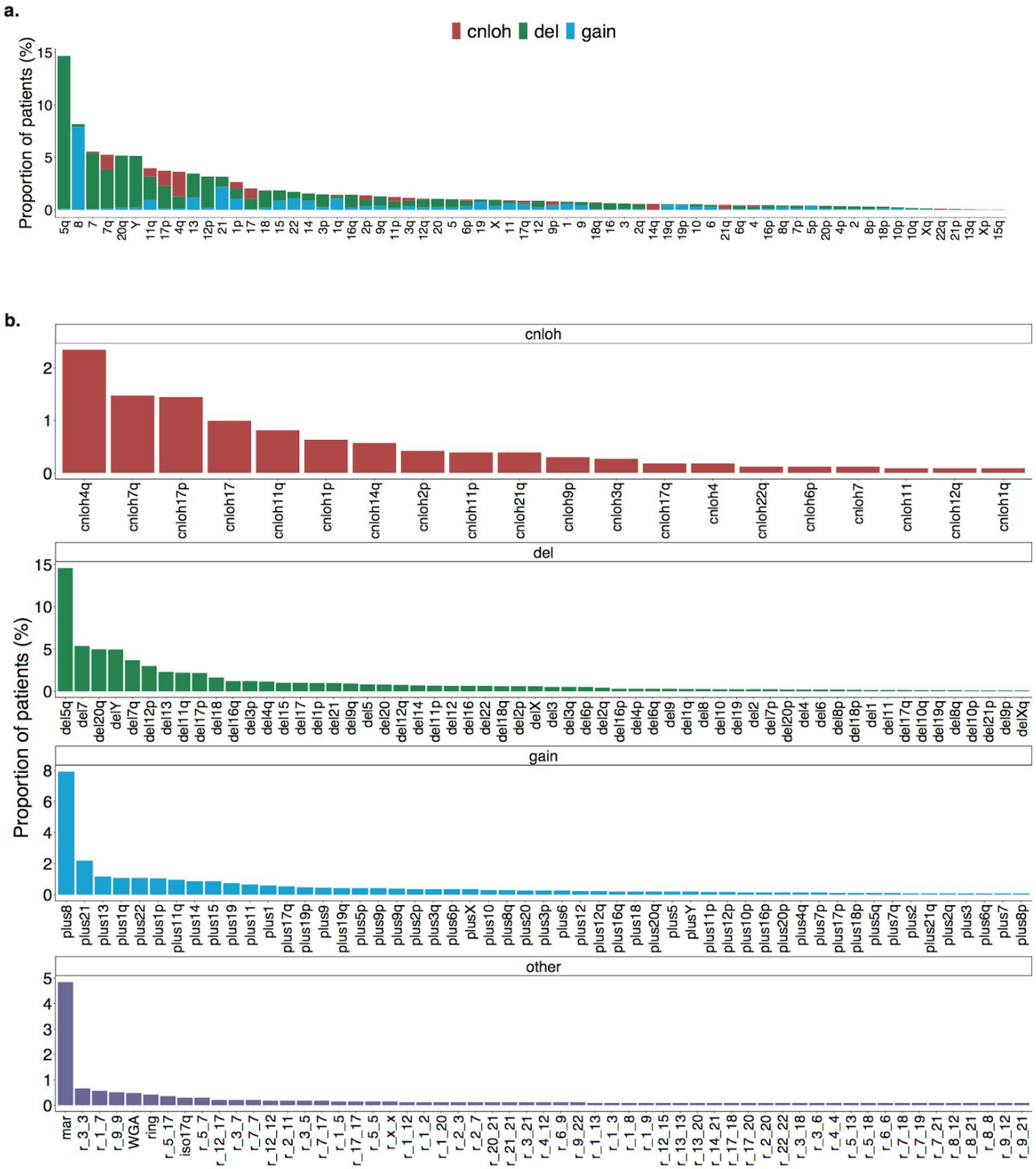
a.
cnloh
del
gain
Proportion of patients (%)
b.
cnloh
del
gain
other
Proportion of patients (%)

Extended Data Figure 2 | Evidence of bi-allelic *TP53* targeting in the cases with multiple *TP53* hits. **a.** Scatter plot of the two maximum *TP53* variant allele frequency (VAF) values from cases with multiple *TP53* mutations and no copy-neutral loss-of-heterozygosity or deletion at *TP53* locus (N=90). Points are annotated according to the level of information of the mutation pairs. In 67% (N=60) of pairs the sum of the two VAFs exceeded 50% so that the mutations were considered to be in the same cells as per the *pigeonhole principle* (triangle and diamond points). In 18 cases, the genomic distance between two mutations was within sequencing read length and it was therefore possible to phase the mutations. In all those cases the mutations were observed to be unphased, i.e., *in trans* (square and diamond points). Within those 18 pairs of unphased mutations, 10 pairs had a sum of VAFs above 50%, i.e., mutations were necessarily on different alleles and in the same cells, implying bi-allelic targeting (diamond points). **b-c.** Scatter plots of the VAF of *TP53* mutations and minor allele frequency of 17p heterozygous SNPs from cases with both a *TP53* mutation and 17p deletion (b.) or 17p copy-neutral LOH (c.). Of note, the high correlations in (a.), (b.) and (c.) (R^2 of 0.77, 0. 94 and 0.97, respectively) are indicative of bi-allelic targeting of *TP53.* **d.** Table of pairs of *TP53* mutations from the same patients that could be phased. All pairs were *in trans*, i.e., mutations were supported by different alleles. **e.** Representative IGV example of unphased mutations (patient p12 from table (b.)).

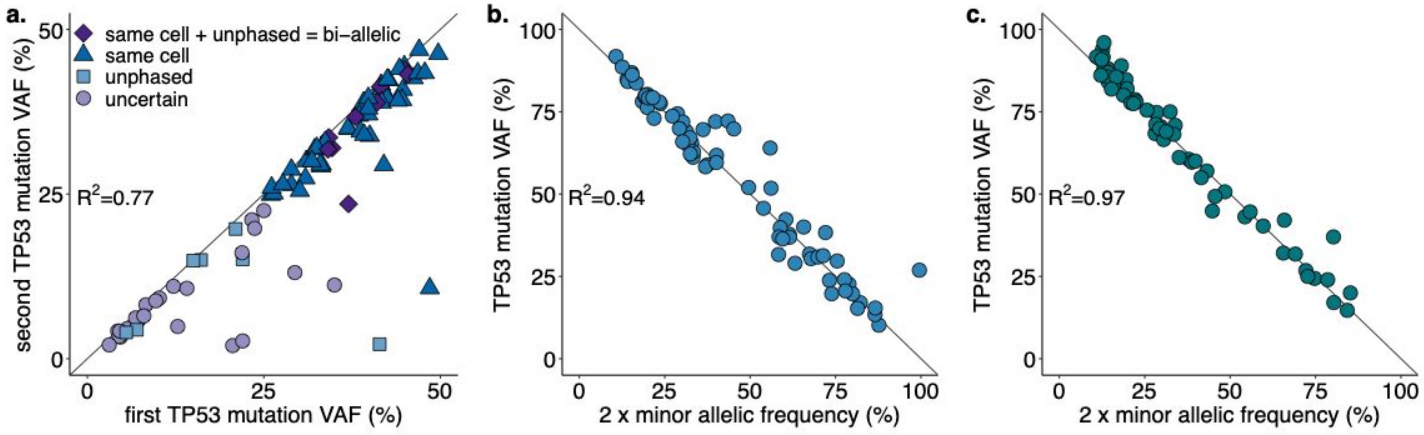

d.

Patient	TP53 Variant 1	Protein Change 1	VAF 1	TP53 Variant 2	Protein Change 2	VAF 2	note
p1	17_7577498_C_T	p.?	0.37	17_7577529_A_T	p.I251N	0.24	
p2	17_7578176_C_T	p.?	0.22	17_7578190_T_C	p.Y220C	0.15	
p3	17_7577538_C_T	p.R248Q	0.16	17_7577570_C_T	p.M237I	0.04	third splice-site mutation at VAF 0.16
p4	17_7577498_C_T	p.?	0.21	17_7577515_T_G	p.T256P	0.2	
p5	17_7577520_A_T	p.I254N	0.46	17_7577539_G_A	p.R248W	0.43	
p6	17_7577106_G_C	p.P278A	0.41	17_7577120_C_T	p.R273H	0.02	
p7	17_7578190_T_C	p.Y220C	0.34	17_7578268_A_C	p.L194R	0.34	
p8	17_7577536_T_A	p.R249W	0.39	17_7577568_C_T	p.C238Y	0.41	
p9	17_7578442_T_C	p.Y163C	0.39	17_7578538_T_A	p.N131I	0.38	
p10	17_7579312_C_T	p.T125T	0.15	17_7579349_A_C	p.F113C	0.15	
p11	17_7578392_C_A	p.E180*	0.05	17_7578403_C_T	p.C176Y	0.06	
p12	17_7578190_T_C	p.Y220C	0.45	17_7578191_A_G	p.Y220H	0.44	
p13	17_7577538_C_T	p.R248Q	0.34	17_7577570_C_T	p.M237I	0.32	
p14	17_7578460_A_C	p.V157G	0.15	17_7578478_G_C	p.P151R	0.65	
p15	17_7578455_C_G	p.A159P	0.04	17_7578524_G_C	p.Q136E	0.07	
p16	17_7577018_C_T	p.?	0.38	17_7577097_C_A	p.D281Y	0.37	
p17	17_7578394_T_A	p.H179L	0.42	17_7578415_AC_A	p.V172fs*2	0.41	
p18	17_7579311_C_T	p.?	0.32	17_7579358_CG_C	p.R110fs*13	0.35	

e.

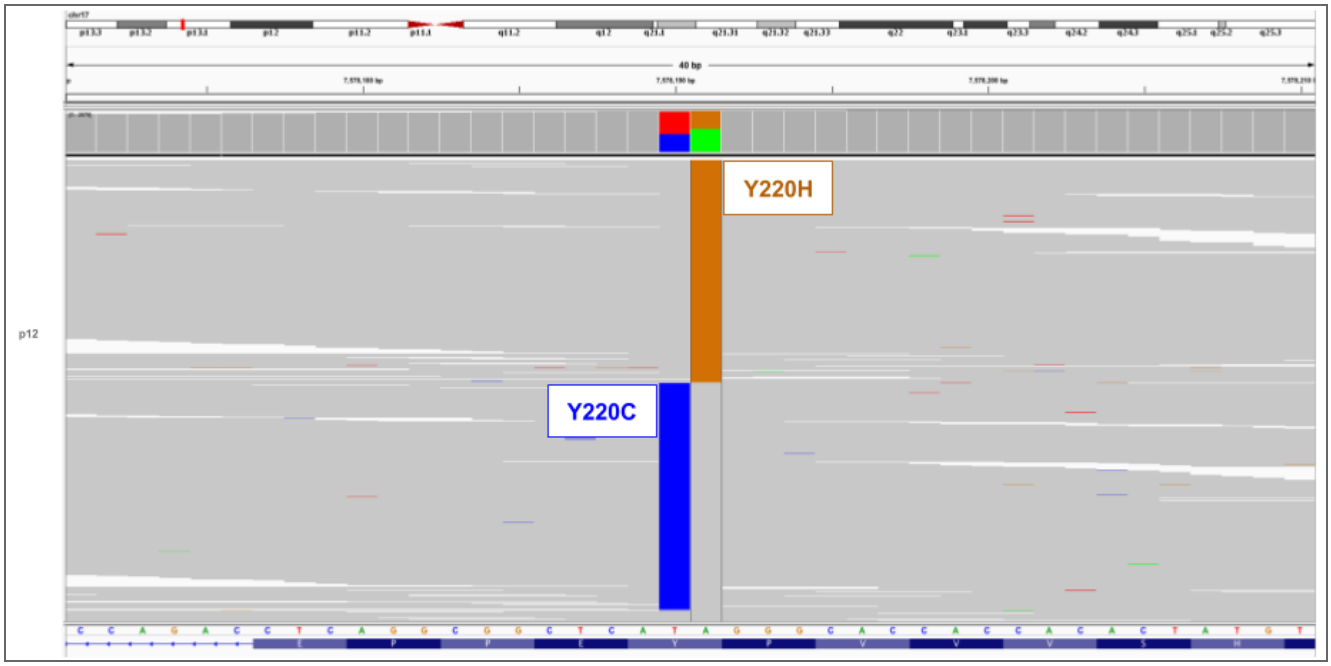

Extended Data Figure 3 | Heatmap of chromosomal aberrations per *TP53* allelic state. Each column represents a patient from the *TP53* subgroups of mono-allelic mutation (top orange band, 1mut), multiple mutations (top light blue band, >1mut), mutation(s) and deletion (top blue band, mut+del) and mutation(s) and copy-neutral loss of heterozygosity (top dark blue band, mut+cnloh). Aberrations observed at a frequency higher than 2% in either mono-allelic or multi-hit *TP53* state are depicted on the y-axis. Aberrations include from top to bottom the annotation of complex karyotype (complex), the presence of marker chromosome (mar), deletion (del), gain (plus), rearrangement (with r_i_j rearrangement between chromosome i and j), copy-neutral loss of heterozygosity (cnloh), whole genome amplification (WGA) and the presence of ring chromosome (ring). Note that the deletions of 17p of two cases from the 1mut *TP53* subgroup did not affect the *TP53* locus.


1mut
>1mut
mut+del
mut+cnloh
complex
mar
del5q/5
del7
del7q
del17p/17
del12p
del13
del18
del20q
del3p
del16q
del21
del15
del4q
del18q
del6p
del22
del16
del12
del9q
del1p
del14
del12q
del11q
del3
del11p
del20
delY
del4p
del3q
delX
del2p
del9
del4
del6q
del16p
del2q
del20p
del2
del19
del10
del8
plus8
plus21
plus1p
plus22
plus11q
plus13
plus15
plus1
plus5p
plus11
plus6p
plus19p
plus9p
plus19q
plus19
plus6
plus8q
plus2p
plus9q
plus17q
plus14
plus3q
plus16q
plus9
plus3p
plus12
r_5_17
r_5_7
r_3_7
r_12_17
cnloh17p/17
cnloh9p
WGA
ring
Aberration
Patient

Extended Data Figure 4 | *TP53* allelic state segregates patient outcomes across WHO subtypes and IPSS-R risk groups. a. Proportion of WHO subtypes per *TP53* allelic state of mono-allelic mutation (1mut) and multiple hits (multi). t-MDS: therapy-related MDS; SLD: single lineage dysplasia; RS: ring sideroblast; MLD: multiple lineage dysplasia; EB: excess blasts; AML-MRC: AML with myelodysplasia-related changes; U: unclassified. Multi-hit *TP53* is enriched for t-MDS compared to mono-allelic *TP53* state (21% vs. 8%, OR=2.9, p=0.002 Fisher exact test) and for MDS-EB2 (31% vs. 13%, OR=3.1, $p<10^{-4}$). Contrarily, mono-allelic *TP53* is enriched for MDS-del5q (15% vs. 2%, OR=8.4, $p<10^{-5}$). **b.** Proportion of IPSS-R risk groups per *TP53* allelic state. Multi-hit *TP53* is strongly enriched for the very-poor category compared to mono-allelic *TP53* state (74% vs. 9%, OR=27, $p<10^{-16}$). **c.** Kaplan-Meier probability estimates of overall survival across main WHO subtypes per *TP53* allelic state of wild-type *TP53* (WT), mono-allelic *TP53* (1mut) and multiple *TP53* hits (multi). WHO subtypes MDS-SLD and MDS-MLD are merged together as MDS-SLD/MLD and WHO subtypes MDS-EB1 and MDS-EB2 are merged together as MDS-EB1/2. **d.** Kaplan-Meier probability estimates of overall survival across IPSS-R risk groups per *TP53* allelic state. IPSS-R very-good and good risk groups are merged together (leftmost panel), and IPSS-R very-poor and poor risk groups are merged together as well (rightmost panel). Annotated p-values are from the log-rank test.

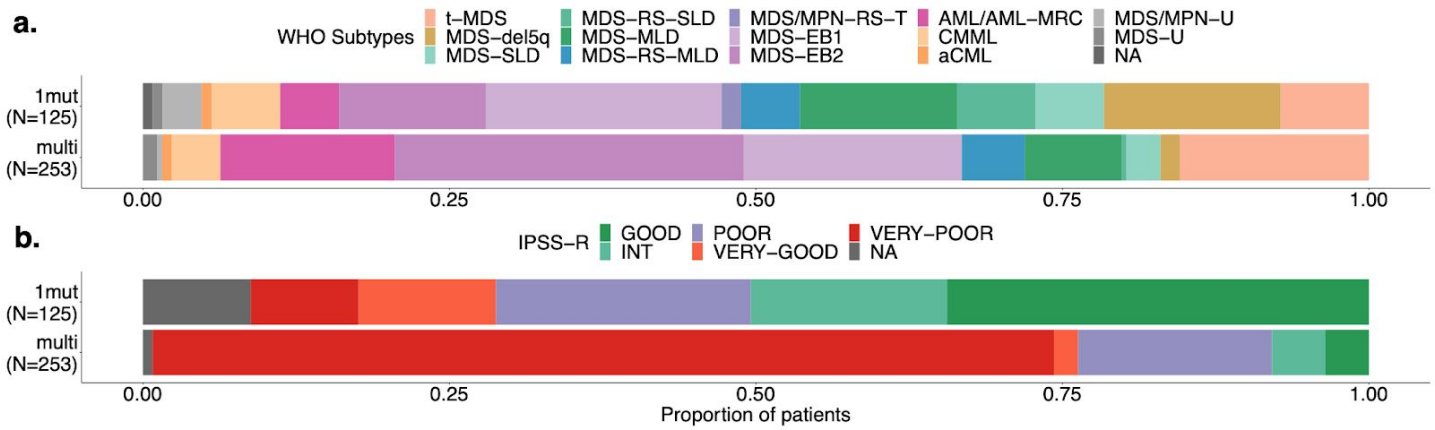
a.
WHO Subtypes
t–MDS
MDS–del5q
MDS–SLD
MDS–RS–SLD
MDS–MLD
MDS–RS–MLD
MDS/MPN–RS–T
MDS–EB1
MDS–EB2
AML/AML–MRC
CMML
aCML
MDS/MPN–U
MDS–U
NA
1mut (N=125)
multi (N=253)
0.00
0.25
0.50
0.75
1.00
b.
IPSS–R
GOOD
INT
POOR
VERY–GOOD
VERY–POOR
NA
1mut (N=125)
multi (N=253)
0.00
0.25
0.50
0.75
1.00
Proportion of patients

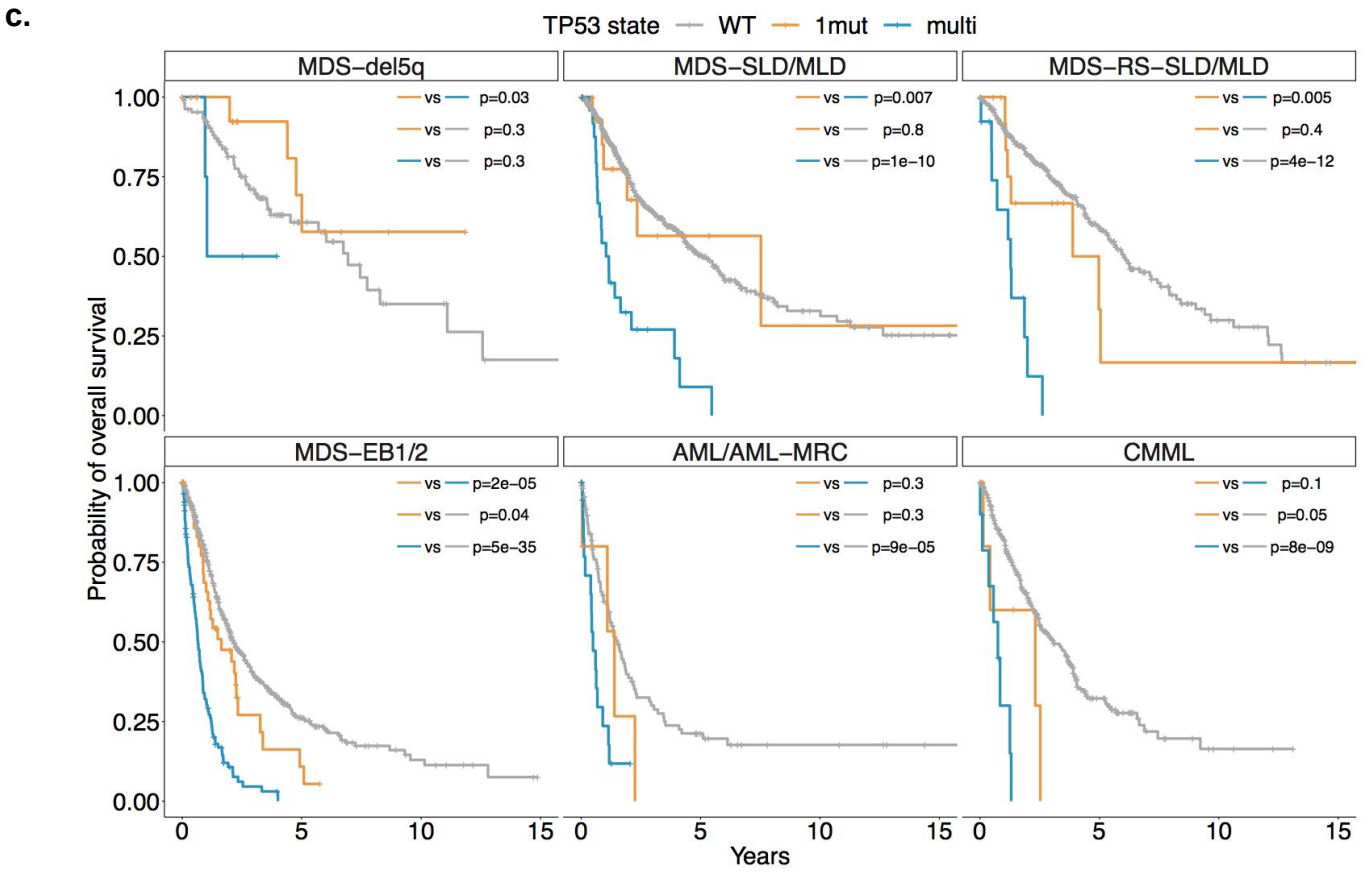
c.
TP53 state
WT
1mut
multi
MDS–del5q
vs p=0.03
vs p=0.3
vs p=0.3
MDS–SLD/MLD
vs p=0.007
vs p=0.8
vs p=1e–10
MDS–RS–SLD/MLD
vs p=0.005
vs p=0.4
vs p=4e–12
MDS–EB1/2
vs p=2e–05
vs p=0.04
vs p=5e–35
AML/AML–MRC
vs p=0.3
vs p=0.3
vs p=9e–05
CMML
vs p=0.1
vs p=0.05
vs p=8e–09
Probability of overall survival
0.00
0.25
0.50
0.75
1.00
0
5
10
15
Years

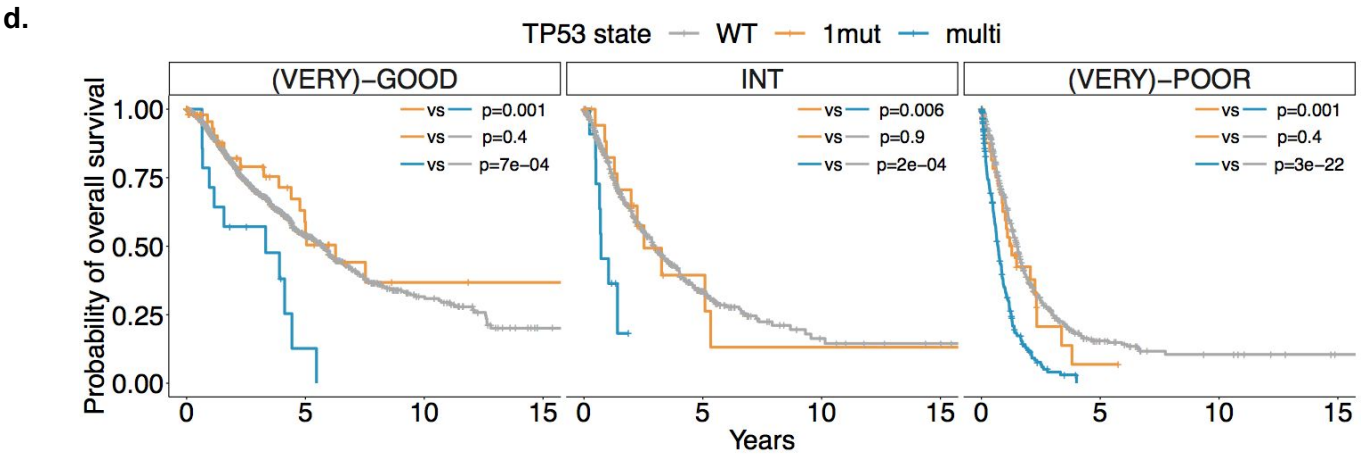
d.
TP53 state
WT
1mut
multi
(VERY)–GOOD
vs p=0.001
vs p=0.4
vs p=7e–04
INT
vs p=0.006
vs p=0.9
vs p=2e–04
(VERY)–POOR
vs p=0.001
vs p=0.4
vs p=3e–22
Probability of overall survival
0.00
0.25
0.50
0.75
1.00
0
5
10
15
Years

Extended Data Figure 5 | Outcomes across *TP53* subgroups and VAF strata. a-b. Kaplan-Meier probability estimates of overall survival (a.) and cumulative incidence of AML transformation (AMLt) (b.) across *TP53* subgroups of wild-type *TP53* (WT), single *TP53* mutation (1mut), multiple *TP53* mutations (>1mut), *TP53* mutation(s) and deletion (mut+del), *TP53* mutation(s) and copy-neutral loss of heterozygosity (mut+cnloh). **c-d,** Kaplan-Meier probability estimates of overall survival (c.) and cumulative incidence of AMLt (d.) per *TP53* allelic state and range of variant allele frequency (VAF) of *TP53* mutations. Annotated p-values are from the log-rank test in (a.) and (c.) and from Gray's test in (b.) and (d.). Numbers in parentheses indicated in the legends represent cases with outcome data.

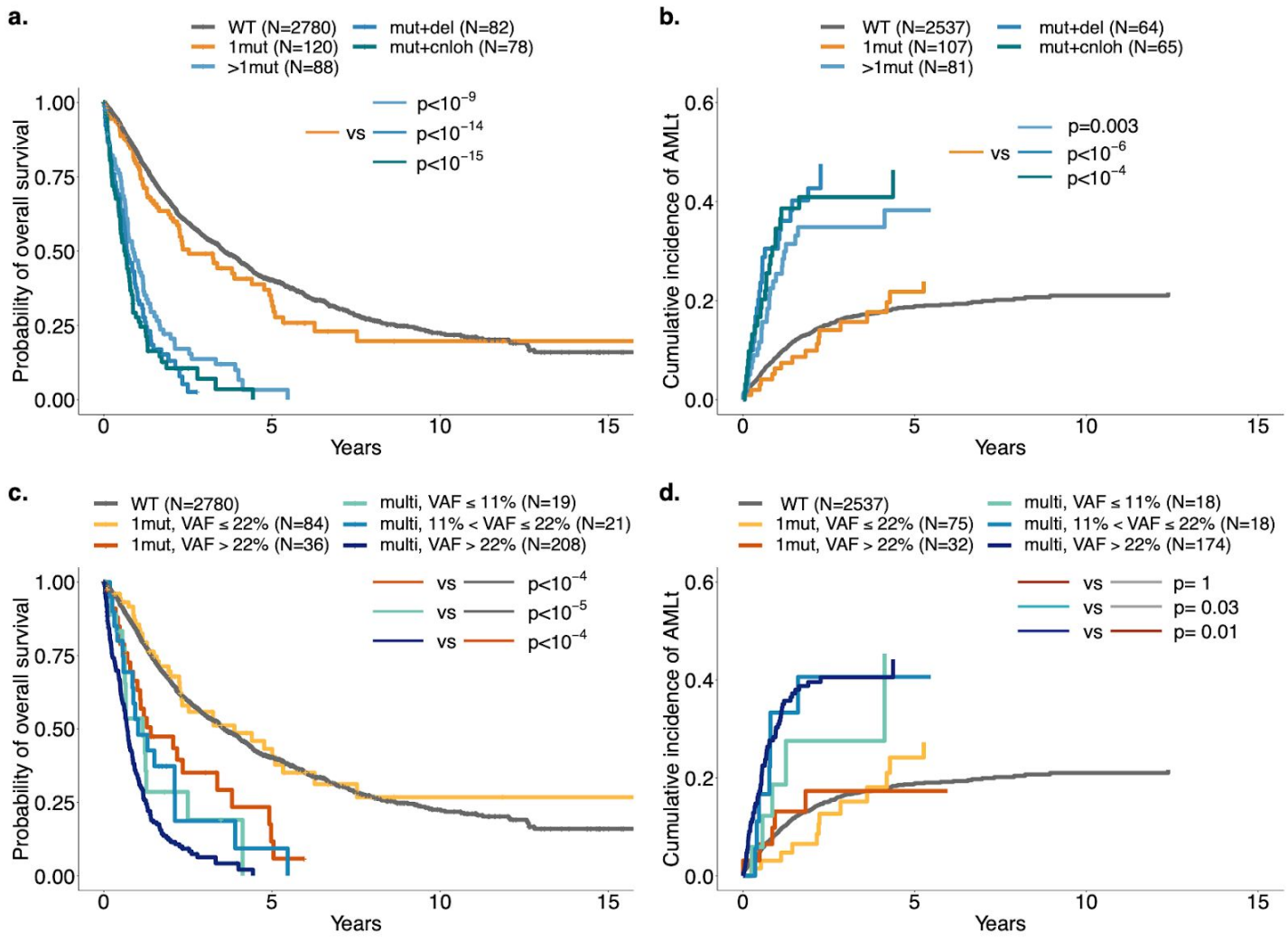
a.
WT (N=2780)
1mut (N=120)
>1mut (N=88)
mut+del (N=82)
mut+cnloh (N=78)
vs
p<10−9
p<10−14
p<10−15
Probability of overall survival
1.00
0.75
0.50
0.25
0.00
0
5
10
15
Years
b.
WT (N=2537)
1mut (N=107)
>1mut (N=81)
mut+del (N=64)
mut+cnloh (N=65)
vs
p=0.003
p<10−6
p<10−4
Cumulative incidence of AMLt
0.6
0.4
0.2
0.0
0
5
10
15
Years
c.
WT (N=2780)
1mut, VAF ≤ 22% (N=84)
1mut, VAF > 22% (N=36)
multi, VAF ≤ 11% (N=19)
multi, 11% < VAF ≤ 22% (N=21)
multi, VAF > 22% (N=208)
vs
p<10−4
vs
p<10−5
vs
p<10−4
Probability of overall survival
1.00
0.75
0.50
0.25
0.00
0
5
10
15
Years
d.
WT (N=2537)
1mut, VAF ≤ 22% (N=75)
1mut, VAF > 22% (N=32)
multi, VAF ≤ 11% (N=18)
multi, 11% < VAF ≤ 22% (N=18)
multi, VAF > 22% (N=174)
vs
p= 1
vs
p= 0.03
vs
p= 0.01
Cumulative incidence of AMLt
0.6
0.4
0.2
0.0
0
5
10
15
Years

Extended Data Figure 6 | Maintained differences in genome instability levels and outcomes between *TP53* states per mutation type. a. Proportion of mutation types across *TP53* subgroups. Truncated mutations (pink) include frameshift indels, nonsense or nonstop mutations and splice-site variants. Mutations annotated as hotspot (purple) are missense mutations at amino acid positions 273, 248, 220 and 175. Mutations annotated as other-missense (green) are additional missense mutations or inframe indels. Odds ratio and Fisher's test p-values for the proportion of truncated versus non-truncated mutations between the multi-hit *TP53* subgroups and the mono-allelic *TP53* subgroup (1mut) are indicated. **b.** Distribution of the number per patient of unique chromosomes other than 17 with aberrations per *TP53* subgroup of single gene mutation (1mut), mutation and deletion (mut+del) and mutation and copy-neutral loss of heterozygosity (mut+cnloh) and across mutation types. Note that 5 patients with both several mutations and deletion or cnloh with ambiguity between the mutation type categories have been excluded for this analysis. ****$p<0.0001$, Wilcoxon rank-sum test, each compared to the same aberration within the 1mut group. **c.** Kaplan-Meier probability estimates of overall survival per *TP53* subgroup across mutation types. Annotated p-values are from the log-rank test.

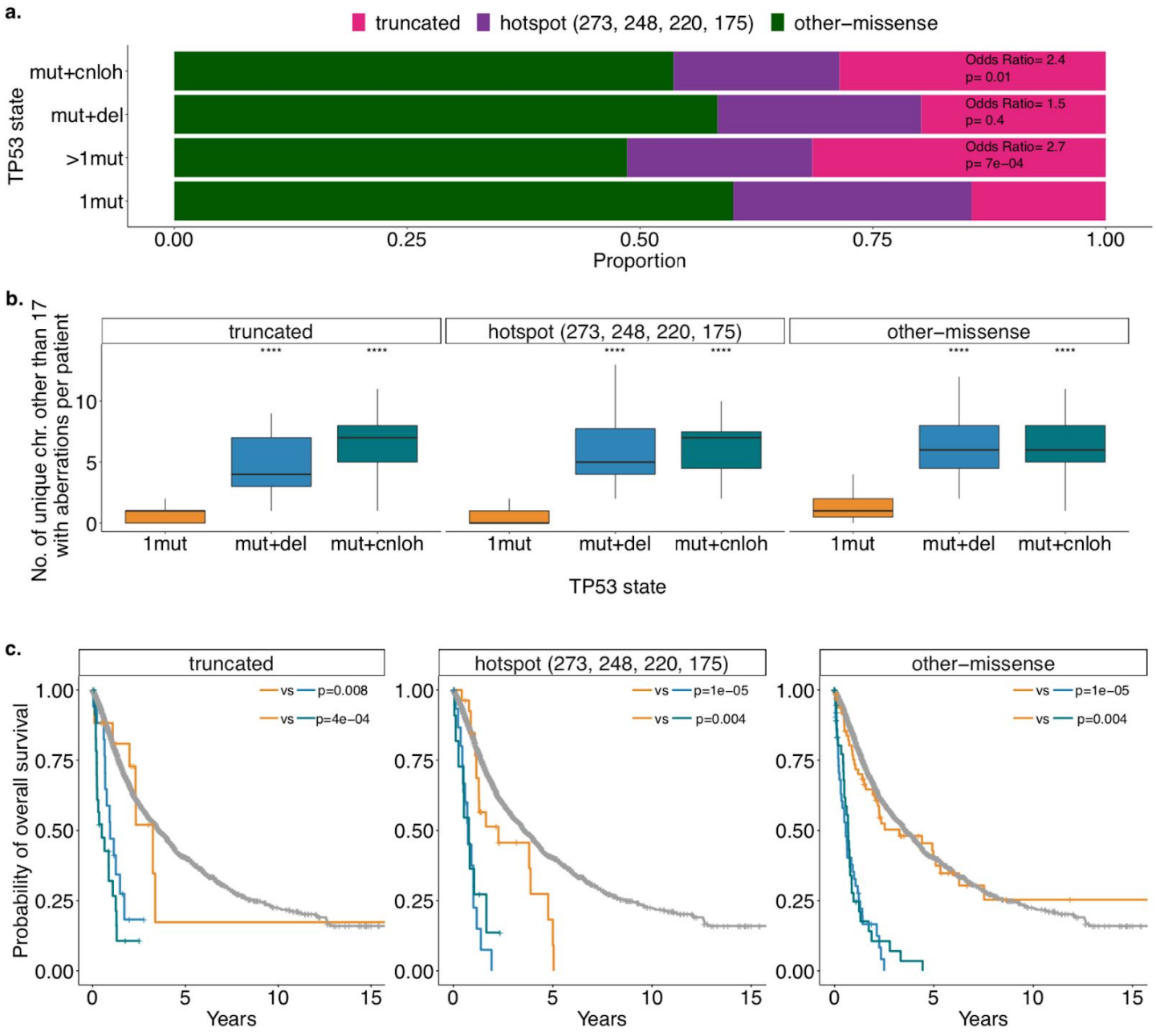
a.
truncated
hotspot (273, 248, 220, 175)
other−missense
TP53 state
mut+cnloh
mut+del
>1mut
1mut
Odds Ratio= 2.4
p= 0.01
Odds Ratio= 1.5
p= 0.4
Odds Ratio= 2.7
p= 7e−04
0.00
0.25
0.50
0.75
1.00
Proportion
b.
truncated
hotspot (273, 248, 220, 175)
other−missense
No. of unique chr. other than 17 with aberrations per patient
****
0
5
10
1mut
mut+del
mut+cnloh
TP53 state
c.
truncated
hotspot (273, 248, 220, 175)
other−missense
Probability of overall survival
vs p=0.008
vs p=4e−04
vs p=1e−05
vs p=0.004
vs p=1e−05
vs p=0.004
0.00
0.25
0.50
0.75
1.00
0
5
10
15
Years

Extended Data Figure 7 | Clinical workflow for the assessment of *TP53* allelic state. Schematic of a simple clinical workflow based on the number of *TP53* mutations, the presence or absence of deletion 17p per cytogenetic analysis, and the presence or absence of cnLOH or focal deletion at 17p per NGS based assay or SNP array. Mutations were considered if VAF≥2%. VAF: variant allele frequency; CK: complex karyotype; OS: overall survival; AML: transformation to acute myeloid leukemia.

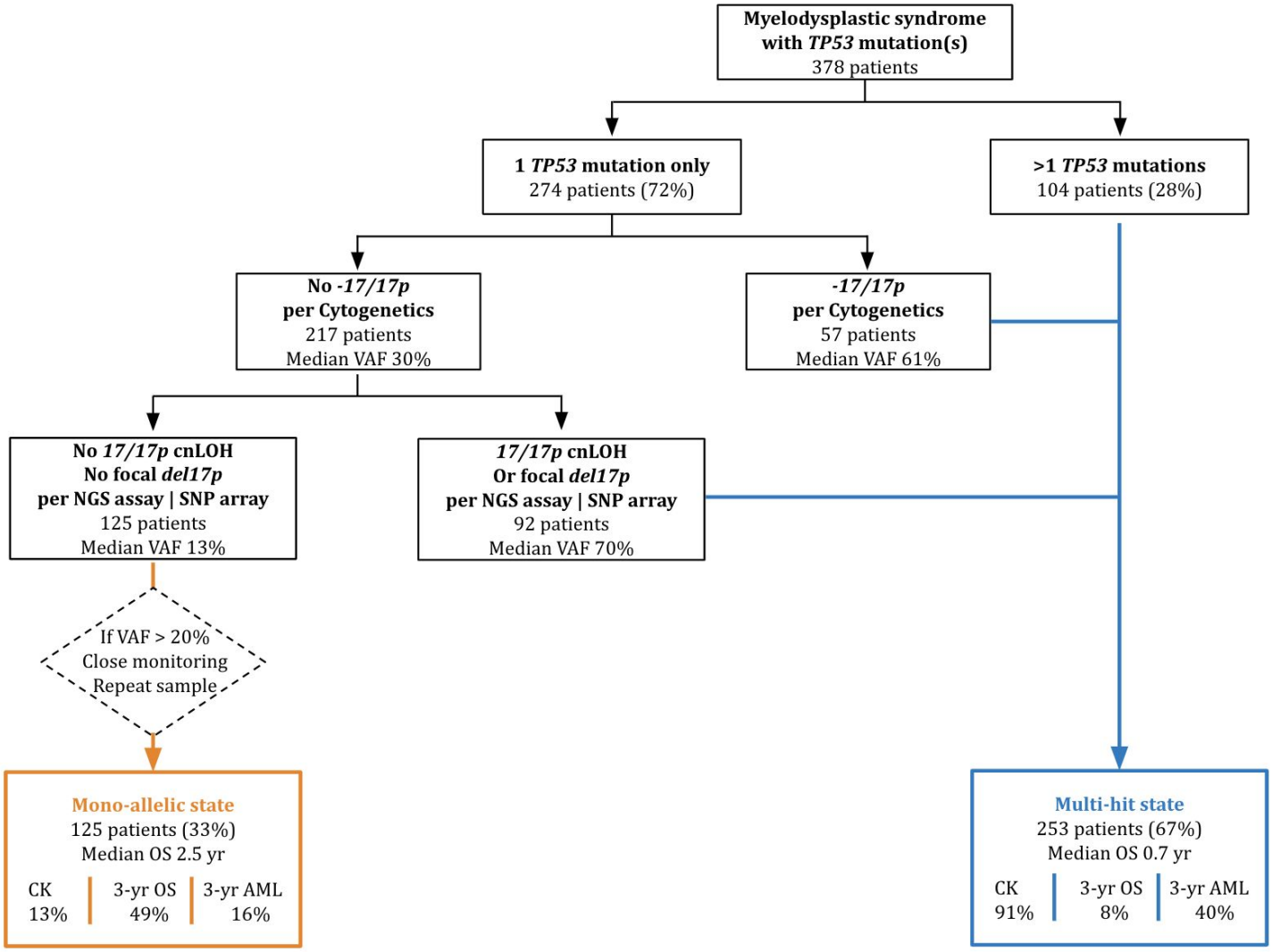
Myelodysplastic syndrome with TP53 mutation(s)
378 patients
1 TP53 mutation only
274 patients (72%)
>1 TP53 mutations
104 patients (28%)
No -17/17p per Cytogenetics
217 patients
Median VAF 30%
-17/17p per Cytogenetics
57 patients
Median VAF 61%
No 17/17p cnLOH
No focal del17p
per NGS assay | SNP array
125 patients
Median VAF 13%
17/17p cnLOH
Or focal del17p
per NGS assay | SNP array
92 patients
Median VAF 70%
If VAF > 20%
Close monitoring
Repeat sample
Mono-allelic state
125 patients (33%)
Median OS 2.5 yr
CK 13%
3-yr OS 49%
3-yr AML 16%
Multi-hit state
253 patients (67%)
Median OS 0.7 yr
CK 91%
3-yr OS 8%
3-yr AML 40%

Extended Data Table 1 | Study cohort characteristics. Table describing the baseline characteristics of the study cohort. 1Q: first quartile; 3Q: third quartile; #: AML classification per WHO 2016 and previously RAEB-T cases. $: Median follow-up time is calculated for censored patients.

IWG-MDS cohort (N=3324)		
Characteristic	**No. of cases (%)**	**Median (1Q - 3Q)**
Gender		
Male	2005 (60%)	-
Female	1319 (40%)	-
Age at diagnosis	-	71 (63 - 78)
Missing data	85 (2.6%)	-
Type of MDS		
De-novo	2855 (86%)	-
Therapy-related	229 (7%)	-
Secondary	51 (1%)	-
Missing data	189 (6%)	-
WHO 2016 classification		
MDS		
MDS-del5q	142 (4.3%)	-
MDS-SLD/MLD	914 (27.5%)	-
MDS-RS-SLD/MLD	460 (13.8%)	-
MDS-EB1	451 (13.6%)	-
MDS-EB2	429 (12.9%)	-
MDS-U	92 (2.8%)	-
AML		
AML-MRC	103 (3%)	-
AML[#]	64 (2%)	-
MDS/MPN		
CMML	425 (12.8%)	-
aCML	46 (1.4%)	-
MDS/MPN-U	50 (1.5%)	-
MDS/MPN-RS-T	42 (1.3%)	-
Other	11 (0.3%)	-
Missing data	95 (2.9%)	-
Cytogenetics IPSS-R		
Very-good	125 (3.8%)	-
Good	1992 (59.9%)	-
Int	421 (12.7%)	-
Poor	149 (4.5%)	-
Very-poor	254 (7.6%)	-
Missing data	383 (11.5%)	-
IPSS-R risk group		
Very-good	372 (14.6%)	-
Good	1106 (33.3%)	-
Int	630 (19%)	-
Poor	448 (13.5%)	-
Very-poor	372 (11.2%)	-
Missing data	282 (8.5%)	-
Blood counts		
Hemoglobin (g/dL)	-	9.7 (8.6 - 11.2)
Platelets (10^9/L)	-	123 (65 - 229)
ANC (10^9/L)	-	2 (1 - 3.7)
Bone Marrow Blasts %	-	3 (1 - 8)
Missing data	108 (3.2%)	-
Outcome		
Median follow-up (years)[$]	-	3.44
Missing OS data	152 (4.5%)	-
Missing AML data	163 (4.9%)	-

Extended Data Table 2 | Validation cohort characteristics. Table describing the baseline characteristics of the validation cohort. 1Q: first quartile; 3Q: third quartile; $: Median follow-up time is calculated for censored patients.

Validation cohort (N=1120)		
Characteristic	**No. of cases (%)**	**Median (1Q - 3Q)**
Cohort		
Clinical sequencing	627 (56%)	-
JMPD	314 (28%)	-
JALSG MDS212	179 (16%)	-
Gender		
Male	751 (67%)	-
Female	369 (33%)	-
Age at diagnosis	-	65 (54 - 75)
Missing data	121 (11%)	-
WHO 2016 classification		
MDS		
t-MDS	9 (0.9%)	-
MDS-del5q	7 (0.6%)	-
MDS-SLD	169 (15.1%)	-
MDS-MLD	100 (8.9%)	-
MDS-RS-SLD/MLD	34 (3%)	-
MDS-EB1/2	437 (39%)	-
MDS-U	15 (1.3%)	-
AML		
AML-MRC	121 (10.8%)	-
MDS/MPN		
CMML	43 (3.8%)	-
aCML	4 (0.4%)	-
MDS/MPN-U	6 (0.5%)	-
MDS/MPN-RS-T	4 (0.4%)	-
Missing data	171 (15.3%)	-
IPSS-R risk group		
Very-good	22 (4.2%)	-
Good	60 (11.4%)	-
Int	77 (14.6%)	-
Poor	101 (19.1%)	-
Very-poor	166 (31.4%)	-
Missing data	102 (19.3%)	-
Blood counts		
Hemoglobin (g/dL)	-	8.4 (7.4 - 10.0)
Platelets (10^9/L)	-	76 (39 - 138)
ANC (10^9/L)	-	1.2 (0.5 - 2.4)
Bone Marrow Blasts %	-	6.8 (2 - 15)
Missing data	554 (49%)	-
Outcome		
Median follow-up (years)[$]	-	1.1
Missing OS data	241 (22%)	-

Extended Data Table 3 | Characteristics of treated cohort subsets. Table describing the baseline characteristics of the subset of patients that i) received hypomethylating agent (HMA), ii) received Lenalidomide in the context of del(5q) or iii) underwent hematopoietic stem cell transplantation (HSCT).

Treated cohort subsets			
	HMA cohort (N=656)	**Lenalidomide cohort (N=101)**	**HSCT cohort (N=310)**
Characteristic	**No. of cases (%)**		
TP53 allelic state			
Wild type	511 (78%)	72 (73%)	274 (88%)
Mono-allelic	24 (4%)	12 (12%)	7 (2%)
Multi-hit	121 (18%)	17 (15%)	29 (9%)
TP53 allelic state, with outcome data			
Wild type	497	69	265
Mono-allelic	22	10	7
Multi-hit	119	16	24
Gender			
Male	428 (65%)	35 (35%)	188 (61%)
Female	228 (35%)	66 (65%)	122 (39%)
WHO 2016 classification			
MDS-del5q	4 (0.6%)	50 (50%)	5 (1.6%)
MDS-SLD/MLD	84 (13%)	3 (3%)	59 (19%)
MDS-RS-SLD/MLD	31 (5%)	3 (2%)	21 (6.6%)
MDS-EB1/2	351 (54%)	28 (28%)	144 (46%)
MDS-U	6 (1%)	4 (4%)	7 (2%)
AML/AML-MRC	63 (10%)	6 (7%)	26 (9%)
MDS/MPN	113 (17%)	6 (6%)	45 (14%)
Missing data	4 (0.6%)	1 (0.9%)	3 (0.9%)
Cytogenetics IPSS-R			
Very-good	11 (2%)	-	3 (0.9%)
Good	340 (51%)	63 (63%)	177 (56%)
Int	100 (16%)	6 (6%)	46 (15%)
Poor	58 (9%)	3 (3%)	35 (11%)
Very-poor	111 (17%)	18 (18%)	25 (9%)
Missing data	36 (5%)	11 (11%)	24 (8%)
IPSS-R risk group			
Very-good	19 (3%)	3 (3%)	11 (3%)
Good	95 (14%)	44 (44%)	60 (19%)
Int	151 (23%)	25 (25%)	89 (28%)
Poor	199 (30%)	7 (7%)	87 (28%)
Very-poor	163 (25%)	17 (17%)	50 (17%)
Missing data	29 (4%)	5 (5%)	13 (4%)